A multiscale extended finite element method for crack propagation

Pierre-Alain Guidault, Olivier Allix, Laurent Champaney, Christian Cornuault

A multiscale extended finite element method for crack propagation

P.-A. Guidault [a,*], O. Allix [a], L. Champaney [a], C. Cornuault [b]

[a] LMT-Cachan (ENS Cachan, CNRS-UMR 8535, Université Pierre et Marie Curie-Paris 6), 61 avenue du Président Wilson, Cachan F-94235, France
[b] Dassault Aviation, 78 quai Marcel Dassault, Saint-Cloud F-92552, France

In this paper, we propose a multiscale strategy for crack propagation which enables one to use a refined mesh only in the crack's vicinity where it is required. Two techniques are used in synergy: a multiscale strategy based on a domain decomposition method to account for the crack's global and local effects efficiently, and a local enrichment technique (the X-FEM) to describe the geometry of the crack independently of the mesh. The focus of this study is the avoidance of meshing difficulties and the choice of an appropriate scale separation to make the strategy efficient. We show that the introduction of the crack's discontinuity both on the microscale and on the macroscale is essential for the numerical scalability of the domain decomposition method to remain unaffected by the presence of a crack. Thus, the convergence rate of the iterative solver is the same throughout the crack's propagation.

Keywords: Multiscale strategy; Crack propagation; X-FEM; Homogenization; LATIN method; Macroenrichment

1. Introduction

In order to verify the tolerance of aeronautical structures to fatigue damage, one needs to investigate the behavior of existing cracks in the structure. The estimation of the velocity of these cracks enables one to evaluate the residual strength of the structure and determine inspection intervals and required maintenance steps. Accounting for the effect of a crack on the response of a structure involves several difficulties. In practice, engineers prefer not to have to change the initial mesh of the structure (that which was defined during the design process), whose element size is sufficient to calculate the global response, but is usually too coarse to represent the local phenomena induced by a crack or even the geometry of the crack itself. Thus, it is necessary to refine the mesh in the potentially cracked area. If the refined mesh is compatible with the coarse mesh, it can be defined as a superelement through static condensation. However, due to the difference in element sizes between the fine mesh and the coarse mesh, the resulting condensed stiffness matrix, when embedded in the global stiffness matrix, may lead to an ill-conditioned system. The multiscale phenomena induced by the crack are not treated efficiently. If the refined mesh and the coarse mesh are not compatible, one can resort to global–local analysis. The displacements (or forces, depending on the method) are extracted from the response of the coarse mesh and prescribed at the boundary of the refined mesh. Then, a local reanalysis is carried out on the refined mesh. The local response is taken into account on the global level by recovering forces (or displacements) at the boundary of this reanalyzed refined zone and applying these to the rest of the coarse mesh. Usually, this process is repeated in order to achieve a correct *global–local dialog* and to obtain a sufficiently accurate solution in the zone of interest. One can mention the works of Hirai [1,2], who combines static condensation techniques and local reanalysis, of Mao and Sun [3], who propose a three-step process (global analysis, local analysis and refined global analysis) and of Whitcomb [4], who presents an iterative strategy. While the last method is

* Corresponding author. Tel.: +33 1 47 40 28 41; fax: +33 1 47 40 22 40.
E-mail address: Pierre-Alain.Guidault@lmt.ens-cachan.fr (P.-A. Guidault).

efficient for local details, such as holes, it may be not suitable when the geometry of this detail evolves, as in the case of a crack. Indeed, the greater the effect of the crack on the global level during its propagation, the more difficult it is to take it into account efficiently. It is necessary to repeat the process many times, which it may be time-consuming.

Besides, the simulation of crack propagation using the finite element method creates meshing difficulties. Today, structural analysis in the presence of cracks is being reconsidered in the light of emerging methods such as the strong discontinuity approach (SDA) introduced by Simo, Oliver and Armero [5–7]. Other approaches, such as the eXtended Finite Element Method (X-FEM) [9–12,14] and the generalized finite element method (G-FEM) [16,17], make use of the partition of unity method (PUM) first introduced by Melenk and Babuška in 1996 [8]. These techniques, by enriching the kinematics of continuous media, enable one to introduce discontinuities into the displacement field with only a relatively small number of degrees of freedom. One of their main advantages is that the mesh does not need to conform to the geometry of the crack. These techniques greatly simplify the meshing and remeshing processes, which despite the progress in meshing tools remain tedious tasks for the engineers confronted with crack propagation problems. However, these techniques do not completely incorporate the multiscale aspect induced by the crack. Usually, they require further remeshing around the crack, particularly at the crack's tip: thus, the remeshing problem is only partially solved. Moreover, for the successful implementation of these enrichment methods, it is essential to control the condition number of the resulting stiffness matrix [28]. One way of doing this is to use suitable preconditioners for the enrichment basis chosen [29]. An alternative, which is developed in this work, consists in treating multiscale phenomena separately.

Here, we propose a two-scale approach in order to address the global–local analysis issue of crack propagation without encountering meshing difficulties. The process involved is a combination of two techniques. The first technique consists in applying the micro–macro approach proposed by Ladevèze [18,19], which is based on a homogenization technique. The microscale is associated with the local phenomena which occur around the crack. This is a much smaller scale than the macroscale, which corresponds to the whole structure. Our two-scale approach ensures the correct global–local interaction between the macroscale and the microscale. The second technique, based on the PUM, is used to define an appropriate representation of the local solution at the crack's tip on the microscale. The introduction of enrichment functions is achieved through the X-FEM. Thus, the multiscale framework enables one to use a suitably refined mesh in the vicinity of the crack's tip while avoiding any constraints of conformity with the coarse mesh which surrounds the refined zone. Moreover, thanks to this scale separation, the macroproblem retains the same structure throughout the calculation while the numerical effort is concentrated on the microlevel [25,26].

In this paper, the integration of the X-FEM into the micro–macro approach is described in detail. In Section 2, the features of the micro–macro approach are presented. This multiscale approach is based on a mixed domain decomposition method. The structure is partitioned into substructures and interfaces. Each of these components has its own variables and its own behavior. Interfaces transfer both force distributions and displacement distributions. Among the various domain decomposition methods, FETI-like dual methods could have been used [21–23], but we preferred a mixed method, which provides a more flexible framework for the integration of the various types of interface behavior (perfect interface, contact interface...). In order to address the global–local analysis issue, one can choose a natural partition based on the distinction between the refined zone and the rest of the structure. Indeed, there is no constraint concerning this choice: nothing would prevent one from choosing a partition based on a coarse finite element mesh (the initial mesh without the crack) in which each coarse element is treated as a substructure. This choice can be made regardless of the crack's configuration. This paper does not detail the way to link nonconforming descriptions (i.e. nonconforming meshes) between the refined substructures in the crack's vicinity and the unrefined substructures. This topic was developed in [25,26]. Let us just mention that an interface link between the local zone and the global zone was proposed in order to transmit forces and moments across the boundary of the refined zone. This link leads to a solution with minimal errors in the zone of interest. The multiscale aspect is introduced only at the interface. The interface quantities (displacements and forces) are split into a macro part and a micro part ($\boldsymbol{q} = \boldsymbol{q}^{\mathrm{M}} + \boldsymbol{q}^{\mathrm{m}}$). The fact that a crack affects both the local level and the global level raises the question of the description of macro and micro quantities. A cubic continuous enrichment of the macrobasis was proposed in [27] in order to take into account the displacement discontinuity when an interface is intersected by a crack. In this paper, a discontinuous macrobasis which is more appropriate for crack modeling is presented.

In Section 3, we describe the iterative solver based on what is known as the LATIN method [24], a nonincremental iterative computational strategy. Each iteration involves the resolution of a linear problem within each substructure and the resolution of a macroproblem. This macroproblem is based on the determination of the homogenized behavior of each substructure. For each substructure, a homogenized operator is built automatically, regardless of the crack's configuration. The properties of this operator are described in the case of a substructure split into two parts by the crack.

The integration of the X-FEM into the micro–macro approach is presented in Section 4. Since the scale separation is introduced only at the interfaces, the determination of an X-FEM approximation for the displacement field in each cracked substructure (subdomain) is easy. Nevertheless, the corresponding discretizations of displacements

and forces at a cracked (i.e. intersected by a crack) interface are developed in detail. The description and propagation of the crack are based on the use of level set functions [30,31] and their application to X-FEM simulations [13,15].

Section 5 deals with the simulation of fatigue crack propagation. The algorithm of the global strategy is presented for this particular situation. The effectiveness of our approach, which we call the MultiScale eXtended Finite Element Method (MS-X-FEM), is illustrated by the propagation of a crack in a plate with three holes subjected to three-point bending. We show that the introduction of the crack's discontinuity on both scales (X-FEM on the microscale and discontinuous macrobasis on the macroscale) leads to good results.

2. Description of the micro–macro approach

Let us consider, assuming small perturbations and an isothermal quasi-static state, the equilibrium of a cracked structure defined in the spatial domain Ω. This structure is subjected to volume forces $\underline{f}_d$ and surface forces $\underline{F}_d$ on a portion $\partial_2\Omega$ of the boundary $\partial\Omega$. On the complementary part $\partial_1\Omega$, the displacement $\underline{u}_d$ is prescribed. The crack is considered to be traction-free.

2.1. Partitioning of the structure into substructures and interfaces

The first step of the strategy consists in describing the structure as an assembly of substructures and interfaces. Each of these components has its own variables and its own equations. A substructure Ω_E, $E \in \boldsymbol{E}$ is subjected to the action of its environment (the neighboring interfaces), defined by a distribution of forces $\underline{F}_E$ and a distribution of displacements $\underline{W}_E$. An interface $\Gamma_{EE'}$ between two substructures Ω_E and $\Omega_{E'}$ generates a constitutive law between the force distributions $(\underline{F}_E, \underline{F}_{E'})$ and the displacement distributions $(\underline{W}_E, \underline{W}_{E'})$ (Fig. 1). Since we are using a mixed domain decomposition method, neither displacement continuity (cf. primal methods) nor the equilibrium of forces (cf. dual methods) is favored at an interface. The displacement, stress and strain fields within a substructure Ω_E are denoted $\underline{u}_E$, σ_E and ε_E respectively.

In practice, interfaces and substructures are discretized in space using classical finite elements. For a substructure, nothing prevents one from using an X-FEM approximation field for the displacements, as will be described in Section 4. At an interface $\Gamma_{EE'}$, the displacements $\underline{W}$ and forces $\underline{F}$ belong to $\mathscr{W}_{EE',h}$ and $\mathscr{F}_{EE',h}$ respectively, where subscript

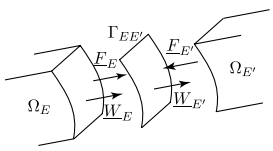

Fig. 1. Interaction among substructures and interfaces.

h designates an approximation space. These spaces are compatible with the force–displacement duality (1)

$$(\underline{F}, \underline{W}) \mapsto \int_{\Gamma_{EE'}} \underline{F} \cdot \underline{W} \, \mathrm{d}\Gamma \tag{1}$$

as well as the following Proposition 1:

Proposition 1. *Spaces $\mathscr{W}_{EE',h}$ and $\mathscr{F}_{EE',h}$ are such that the bilinear form* (1) *is nondegenerate*:

$$\left\{ \underline{F} \in \mathscr{F}_{EE',h}, \int_{\Gamma_{EE'}} \underline{F} \cdot \underline{W} \, \mathrm{d}\Gamma = 0, \forall \underline{W} \in \mathscr{W}_{EE',h} \right\} = \{0\},$$

$$\left\{ \underline{W} \in \mathscr{W}_{EE',h}, \int_{\Gamma_{EE'}} \underline{F} \cdot \underline{W} \, \mathrm{d}\Gamma = 0, \forall \underline{F} \in \mathscr{F}_{EE',h} \right\} = \{0\}.$$

The approximation spaces of $\mathscr{W}_{EE',h}$ and $\mathscr{F}_{EE',h}$ must be chosen carefully. Choosing a wrong discretization for $\mathscr{F}_{EE'}$ could generate spurious oscillating modes leading to numerical instability [32,33]. Let us just mention that ways to avoid this problem include the refinement of the substructure's mesh ("h-version") or the use of a higher degree of approximation p for $\underline{u}_h$ ("p-version") near the boundary, as illustrated in Fig. 2. Suitable boundary bubbles to stabilize this problem are proposed in [34]. Here, we will be using the "h-version" and $\mathscr{W}_{EE',h} = \mathscr{F}_{EE',h}$. Since the substructures are meshed with linear triangles or bilinear quadrilaterals, this leads to spaces $\mathscr{W}_{EE',h}$ and $\mathscr{F}_{EE',h}$ which correspond to a space of piecewise constant functions over $\Gamma_{EE'}$. The definitions of $\mathscr{W}_{EE'}$ and $\mathscr{F}_{EE'}$ are extended to the whole set of interfaces of a substructure Ω_E.

$$\mathscr{F}_E = \prod_{E' \in \mathbf{V}_E} \mathscr{F}_{EE'} \quad \text{and} \quad \mathscr{W}_E = \prod_{E' \in \mathbf{V}_E} \mathscr{W}_{EE'}, \tag{2}$$

where $\mathbf{V}_E$ is the set of the neighboring substructures of Substructure Ω_E. The extension of these definitions to the

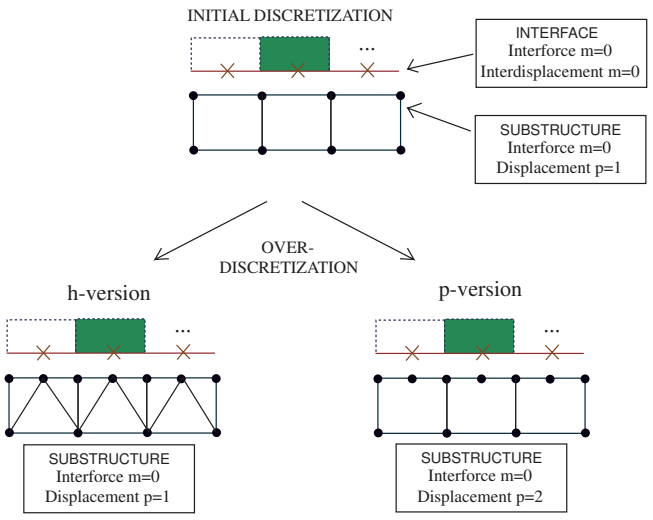

Fig. 2. Modification of the classical approximations of the interforce (FE approximation of degree m) and local displacement along the edge of a substructure (FE approximation of degree p) for finite element calculations: h- and p-versions.

whole set of substructures leads to Spaces $\mathscr{F}$ and $\mathscr{W}$. Let us introduce the following definition:

Definition 1 (E-admissibility). For a substructure E, $s_E = (\varepsilon_E, \underline{W}_E, \sigma_E, \underline{F}_E) \in \mathscr{S}_E$ is said to be E-admissible if it verifies:

- The kinematic admissibility of $(\varepsilon_E, \underline{W}_E)$: $\exists \underline{u}_E \in \mathscr{U}_E$ such that $\varepsilon_E = \varepsilon(\underline{u}_E)$ and

$$\forall \underline{F}^* \in \mathscr{F}_E, \quad \int_{\partial\Omega_E} \underline{F}^* \cdot (\underline{u}_E - \underline{W}_E) \mathrm{d}\Gamma = 0.$$

- The static admissibility of $(\sigma_E, \underline{F}_E)$,

$$\forall \underline{u}^* \in \mathscr{U}_E, \quad \int_{\Omega_E} \sigma_E : \varepsilon(\underline{u}^*) \mathrm{d}\Omega = \int_{\Omega_E} \underline{f}_d \cdot \underline{u}^* \, \mathrm{d}\Omega + \int_{\partial\Omega_E} \underline{F}_E \cdot \underline{u}^* \, \mathrm{d}\Gamma.$$

  The corresponding space is denoted $\mathbf{F}_{E,\mathrm{ad}}$. $\mathbf{F}_{E,\mathrm{ad},0}$ is the associated vector space (for $\underline{f}_d = 0$).
- The constitutive equation $\sigma_E = \boldsymbol{K}{:}\varepsilon_E$ where $\boldsymbol{K}$ is the Hooke's tensor. The corresponding space is designated by $\boldsymbol{S}_{E,\mathrm{ad}}$. $\boldsymbol{S}_{E,\mathrm{ad},0}$ is the associated vector space.

Then, the reference substructured problem can be reformulated as:

Problem 1. Find $\boldsymbol{s} = \{\boldsymbol{s}_E\}_{E \in \mathbf{E}}$, with $\boldsymbol{s}_E = (\varepsilon_E, \underline{W}_E, \sigma_E, \underline{F}_E) \in \mathscr{S}_E$, which verifies:

- the E-admissibility of $s_E \forall E \in \mathbf{E}$,
- the behavior at the interfaces, the boundary conditions over $\partial_1\Omega$ and $\partial_2\Omega$ being considered special cases.

The behavior at the interface depends on the connection which is to be modeled and can been expressed as a mixed constitutive law between the force distributions $(\underline{F}_E, \underline{F}_{E'})$ and the displacement distributions $(\underline{W}_E, \underline{W}_{E'})$. For each interface $\Gamma_{EE'}$, this constitutive law can be formally written at any point $\underline{x}$ of the interface as:

$$R(\underline{W}_E, \underline{F}_E, \underline{W}_{E'}, \underline{F}_{E'}) = 0, \quad \forall \underline{x} \in \Gamma_{EE'}, \tag{3}$$

which in the case of unilateral contact, can be a nonlinear relation [32,37]. For instance, in order to describe the behavior of a perfect connection between Ω_E and $\Omega_{E'}$, relation (3) corresponds simply to the following equations:

$$\underline{W}_E - \underline{W}_{E'} = 0 \quad \text{(displacement continuity)}, \tag{4}$$

$$\underline{F}_E + \underline{F}_{E'} = 0 \quad \text{(equilibrium of forces)}. \tag{5}$$

2.2. Description of quantities on the macroscale and on the microscale

The distinction between the micro and macro levels is made only at the interfaces. Macro fields (superscript M) and micro fields (superscript m) are defined only at the interfaces prior to any discretization. The macroscale is defined by the characteristic length of the interfaces, which is *a priori* greater than the discretization on the microscale. Let us consider a particular interface $\Gamma_{EE'}$ (Fig. 1). We may freely choose the spaces $\mathscr{F}^M_{EE'}$ and $\mathscr{W}^M_{EE'}$ in which the macrodisplacements and macroforces are sought provided that these spaces are compatible with the force–displacement duality (1) and the following proposition:

Proposition 2

$$\left\{ \underline{F}^M \in \mathscr{F}^M_{EE'}, \int_{\Gamma_{EE'}} \underline{F}^M \cdot \underline{W}^{M*} \mathrm{d}\Gamma = 0, \forall \underline{W}^{M*} \in \mathscr{W}^M_{EE'} \right\} = \{0\},$$

$$\left\{ \underline{W}^M \in \mathscr{W}^M_{EE'}, \int_{\Gamma_{EE'}} \underline{F}^{M*} \cdot \underline{W}^M \mathrm{d}\Gamma = 0, \forall \underline{F}^{M*} \in \mathscr{F}^M_{EE'} \right\} = \{0\}.$$

Proposition 2 implies that Spaces $\mathscr{F}^M_{EE'}$ and $\mathscr{W}^M_{EE'}$ have the same dimension. Usually, one chooses for $\underline{W}^{\mathbf{M}}$ and $\underline{F}^{\mathbf{M}}$ affine functions on $\Gamma_{EE'}$, the only constraint being for the space of the macrodisplacements to contain the rigid body modes over $\partial\Omega_E$, so that the multiscale approach is numerically scalable [18,19]. Finally, $\underline{F}^M$ and $\underline{W}^M$ are written over $\Gamma_{EE'}$ in the form $\underline{F}^M = \sum_{i=1}^{n_M} (\underline{F}, \underline{e}^M_i) \underline{e}^M_i = \sum_{i=1}^{n_M} [F^M]_i \underline{e}^M_i$. One possible choice for the macrobasis is represented in Fig. 3. This definition of macroquantities is physically sound: these quantities are mean values with regard to space. They are also the best possible approximations with respect to the work bilinear form (1). Because of Proposition 2, they are uniquely defined.

Definition 2. The macro parts $(\underline{W}^M, \underline{F}^M) \in \mathscr{W}^M_{EE'} \times \mathscr{F}^M_{EE'}$ of $(\underline{W}, \underline{F}) \in \mathscr{W}_{EE'} \times \mathscr{F}_{EE'}$ are defined by the following expressions:

$$\underline{W}^M \in \mathscr{W}^M_{EE'}, \quad \int_{\Gamma_{EE'}} (\underline{W}^M - \underline{W}) \cdot \underline{F}^{M^*} \mathrm{d}\Gamma = 0, \quad \forall \underline{F}^{M^*} \in \mathscr{F}^M_{EE'},$$

$$\underline{F}^M \in \mathscr{F}^M_{EE'}, \quad \int_{\Gamma_{EE'}} (\underline{F}^M - \underline{F}) \cdot \underline{W}^{M^*} \mathrm{d}\Gamma = 0, \quad \forall \underline{W}^{M^*} \in \mathscr{W}^M_{EE'}.$$

Consequently, the micro parts are $\underline{F}^m = \underline{F} - \underline{F}^M$ and $\underline{W}^m = \underline{W} - \underline{W}^M$. Therefore, the scales can be uncoupled as follows:

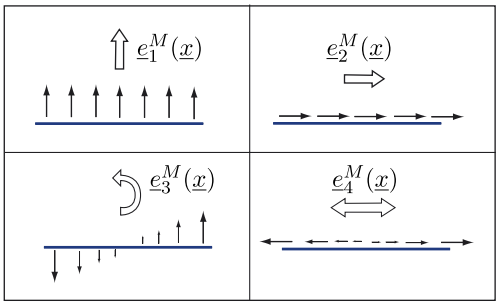

Fig. 3. Linear macrobasis $\{\underline{e}^M_i\}_{k=1..4}$, $(n_M = 4)$, for an interface $\Gamma_{EE'}$.

$$\int_{\Gamma_{EE'}} \underline{F} \cdot \underline{W}\, \mathrm{d}\Gamma = \int_{\Gamma_{EE'}} \underline{F}^M \cdot \underline{W}^M\, \mathrm{d}\Gamma + \int_{\Gamma_{EE'}} \underline{F}^m \cdot \underline{W}^m\, \mathrm{d}\Gamma. \qquad (6)$$

This partitioning, which can be extended to the whole set of interfaces, leads to Spaces $\mathscr{W}^M$, $\mathscr{W}^m$, $\mathscr{F}^M$ and $\mathscr{F}^m$. Let us note that relation (6) is independent of the homogenization technique, which will be presented later.

The choice of a macrobasis described in Fig. 3 may not be suitable for taking the displacement discontinuity induced by a crack into account. A macrobasis which extracts not only the linear part, but also the quadratic and cubic parts of an interface quantity in order to represent the crack's opening at an interface intersected by the crack was proposed in [27]. This cubic macroenrichment enabled us to improve the efficiency of the strategy. Here, we propose a discontinuous macrobasis. Let us consider an interface intersected by a crack at a given point C (Fig. 4). A simple way of building a discontinuous macrobasis consists in using a linear macrobasis (Fig. 3) for each part Γ_1 and Γ_2, which leads to a piecewise linear macrobasis. The macroforces and macrodisplacements on one part of the interface are defined using the vectors of the linear macrobasis and are set to zero on the other part (Fig. 4). Thus, the macrobasis vectors $\underline{e}_1^M(\underline{x})$, $\underline{e}_2^M(\underline{x})$, $\underline{e}_3^M(\underline{x})$ and $\underline{e}_4^M(\underline{x})$ are orthogonal to the four other vectors $\underline{e}_5^M(\underline{x})$, $\underline{e}_6^M(\underline{x})$, $\underline{e}_7^M(\underline{x})$ and $\underline{e}_8^M(\underline{x})$ in the sense of the work bilinear form (1). This leads to an orthogonal macrobasis. From now on, we will refer to this piecewise linear macrobasis as the discontinuous macrobasis.

Let us consider the academic example of a structure with a traction-free crack intersecting an interface (Fig. 5). The macromesh of the interfaces is shown in Fig. 5c and the micromeshes of Substructures Ω_E and $\Omega_{E'}$ are shown in Fig. 5b. The deformed shape and the macrodisplacements $\underline{W}_E^M$ obtained with a linear macrobasis (Fig. 6a) show that, unlike the complementary micro part $\underline{W}_E^m = \underline{W}_E - \underline{W}_E^M$, $\underline{W}_E^M$ is continuous across $\Gamma_{EE'}$. Similar results for a cubic macrobasis are shown in Fig. 6b. Let us observe that according to the definition of the macrobasis at an interface the resulting homogenized behavior of each substructure can take the macroeffect of the crack into account. Thus, the resulting homogenized operator can represent not only homogenous macrostates, but also macro gradient states such as those defined by homogenized operators of the Cosserat [35] or micropolar [36] media types. The use of the discontinuous macrobasis for the interface intersected by the crack is shown in Fig. 7. In this case, the discontinuity induced by the crack is introduced on both levels. The macrodisplacement $\underline{W}_E^M$ and its complementary micro part $\underline{W}_E^m$ are both discontinuous.

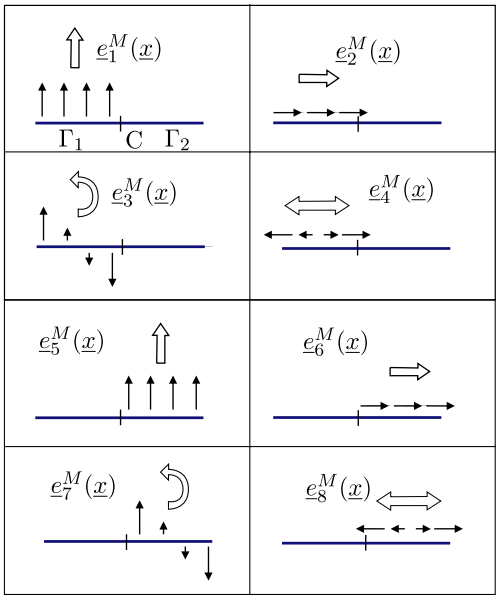

Fig. 4. Discontinuous macrobasis: piecewise linear macrobasis $\{\underline{e}_i^M\}_{i=1..8}$, $(n_M = 8)$, for an interface $\Gamma_{EE'}$ intersected by a crack at midpoint.

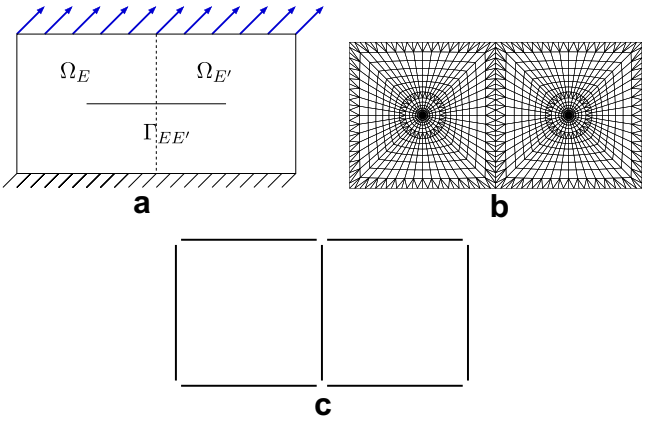

Fig. 5. A structure with a traction-free crack intersecting an interface. (a) Substructures (Ω_E and $\Omega_{E'}$). (b) Micromeshes. (c) Macromesh.

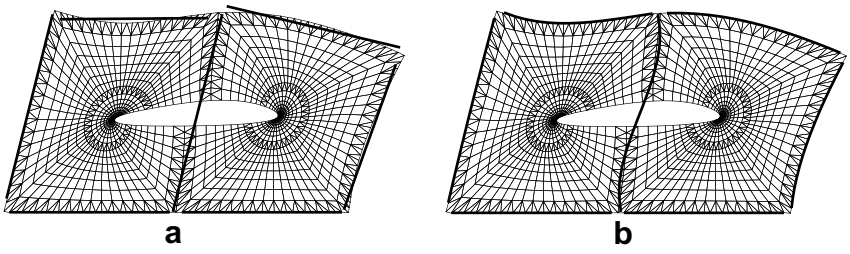

Fig. 6. Deformed shape and macrodisplacements $\underline{W}_E^M$ (thick lines) at the interfaces using a linear macrobasis: the discontinuity is introduced only on the microscale. (a) Linear macrobasis. (b) Cubic macrobasis.

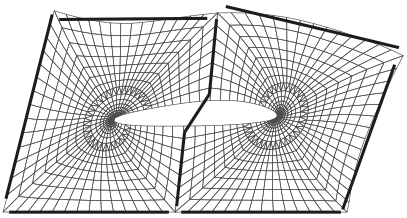

Fig. 7. Deformed shape and macrodisplacements $\underline{W}_E^M$ (thick lines) at the interfaces using a discontinuous macrobasis: the discontinuity is introduced on both the microscale and the macroscale.

Remark 1. The choice of piecewise constant functions as the discretization space for interface quantities (see Section 2.1) enables a discontinuity between the elements of the interface located on the both sides of the crack to be introduced naturally.

Remark 2. The definition of the discontinuous macrobasis requires the position where the crack intersects the interface to be predetermined. This can be cumbersome in the crack propagation situation. The use of a level set function whose zero isovalue defines the intersection point alleviates this difficulty (see Section 4). In the situation where the crack is completely or partially aligned with an interface, a new interface behavior (Eq. (3)) is needed. For example, one can introduce a contact interface. This type of interface behavior is described in [32,37].

2.3. Partial verification of transmission conditions

Another important feature of the multiscale computational strategy is that the transmission conditions at the interfaces are partially verified *a priori*. The macroforces must verify the transmission conditions (i.e. the equilibrium at the interface in terms of the macroforces) systematically, including the boundary conditions. The corresponding space is designated by $\mathscr{F}_{\text{ad}}^M$.

$$\mathscr{F}_{\text{ad}}^M = \{\underline{F}^M \in \mathscr{F}^M | \forall E \in \mathbf{E}, \quad \forall E' \in \mathbf{V}_E, \underline{F}_E^M + \underline{F}_{E'}^M = 0\}. \tag{7}$$

3. A LATIN-based iterative solver

3.1. Principle

The partial verification of the transmission conditions *a priori* at the interfaces leads to the following reformulation of the reference problem: Find $\boldsymbol{s} = \{\boldsymbol{s}_E\}_{E\in\mathbf{E}}$, with $\boldsymbol{s}_E \in \mathscr{S}_E$, which verifies:

$\boldsymbol{A}_d$
- the E-admissibility of $\boldsymbol{s}_E$, $\quad E \in \mathbf{E} : \boldsymbol{s}_E \in \boldsymbol{S}_{E,\text{ad}}$ (see Definition 1),
- the admissibility of $\underline{F}^M : \underline{F}^M \in \mathscr{F}_{\text{ad}}^M$ (see (7)),

$\boldsymbol{\Gamma}$
- the constitutive relation (3) describing the behavior at the interfaces,

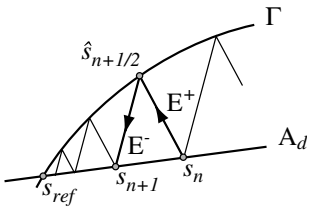

Fig. 8. The LATIN scheme for one iteration.

$\boldsymbol{\Gamma}$constitutes a set of (possibly nonlinear) equations which are local in space. $\boldsymbol{A}_d$ is a set of global linear equations. With this decomposition, it is possible to apply the LATIN method [24], a general computational strategy for time-dependent nonlinear problems which operates globally over the entire space–time domain. Under the assumption of small perturbations and an isothermal quasi-static state, the time does not intervene: in this case, the capabilities of the LATIN method are not fully exploited. Nevertheless, this general method is used here even though such a framework is not required. Other equivalent formulations exist and can be used. Fig. 8 illustrates the procedure for one iteration, which is composed of two stages: the local stage and the linear stage.

Remark 3. The admissibility of the macroforces (Eq. (7)) ensures the propagation of global information throughout the whole set of substructures. The strategy is numerically scalable provided that the macroforces can represent the resultants and moments at the interfaces. This point will be discussed later in the case where a crack is present.

3.2. The local stage at iteration n

The local stage consists in constructing $\hat{\boldsymbol{s}}_{n+1/2} \in \boldsymbol{\Gamma}$ given $\boldsymbol{s}_n \in \boldsymbol{A}_d$ (Fig. 8). $(\hat{\boldsymbol{s}}_{n+1/2} - \boldsymbol{s}_n)$ must follow a search direction E^+. For each interface $\Gamma_{EE'}$, $\hat{\boldsymbol{s}}_{n+1/2}$ must verify:

$$\forall \underline{F}^* \in \mathscr{F}_{EE'},$$
$$\int_{\Gamma_{EE'}} \{k^{-1}(\widehat{\underline{F}}_E - \underline{F}_E) - (\widehat{\underline{W}}_E - \underline{W}_E)\} \cdot \underline{F}^* \, \mathrm{d}\Gamma = 0, \tag{8}$$

where k is a positive scalar. This is a parameter of the method which can be viewed as a micro stiffness coefficient of the interface [33]. The subscripts n and $n+1/2$ have been omitted to simplify the notations. The local step presents no difficulty. This problem is local with respect to the space variable and lends itself well to the highest degree of parallelism. In the case of a perfect interface $\Gamma_{EE'}$, (4) and (5) along with the search direction (8) enable one to express the "hat" interface quantities $\widehat{\underline{W}}_E$, $\widehat{\underline{W}}_{E'}$, $\widehat{\underline{F}}_E$ and $\widehat{\underline{F}}_{E'}$ as functions of the quantities $\underline{W}_E$, $\underline{W}_{E'}$, $\underline{F}_E$ and $\underline{F}_{E'}$ from the previous linear stage. Thus:

$$\forall \underline{x} \in \Gamma_{EE'}, \quad \widehat{\underline{W}}_E = \widehat{\underline{W}}_{E'} = \frac{1}{2}(\underline{W}_E + \underline{W}_{E'}) - \frac{1}{2k}(\underline{F}_E + \underline{F}_{E'}),$$
$$\forall \underline{x} \in \Gamma_{EE'}, \quad \widehat{\underline{F}}_E = -\widehat{\underline{F}}_{E'} = \frac{1}{2}(\underline{F}_E - \underline{F}_{E'}) - \frac{1}{2}k(\underline{W}_E - \underline{W}_{E'}).$$

3.3. The linear stage at iteration n

The linear stage consists in constructing $\boldsymbol{s}_{n+1} \in \boldsymbol{A}_d$ given $\hat{\boldsymbol{s}}_{n+1/2} \in \boldsymbol{\Gamma}$. $(\boldsymbol{s}_{n+1} - \hat{\boldsymbol{s}}_{n+1/2})$ must follow a search direction E. For each substructure Ω_E, $E \in \mathbf{E}$, $\boldsymbol{s}_{n+1}$ must verify:

$$\forall \underline{F}^* \in \mathscr{F}^m \cup \mathscr{F}^M_{\mathrm{ad}},$$

$$\sum\nolimits_{E\in\mathbf{E}} \int_{\partial\Omega_E} \{k^{-1}(\underline{F}_E - \widehat{\underline{F}}_E) + (\underline{W}_E - \widehat{\underline{W}}_E)\} \cdot \underline{F}^*_E \,\mathrm{d}\Gamma = 0, \quad (9)$$

where subscripts $n+1/2$ and $n+1$ have been omitted. The admissibility of $\underline{F} \in \mathscr{F}^M_{\mathrm{ad}}$ is ensured by the introduction of a Lagrange multiplier $\widetilde{\underline{W}}^M \in \mathscr{W}^M_{\mathrm{ad},0}$ [20]. $\mathscr{W}^M_{\mathrm{ad},0}$ corresponds to the space of the macrodisplacements which are continuous across the interfaces and equal to zero along $\partial_1\Omega$. Thus, Eq. (9) can be rewritten as follows:

$$\forall \underline{F}^* \in \mathscr{F}, \quad \sum_{E\in\mathbf{E}} \int_{\partial\Omega_E} \{k^{-1}(\underline{F}_E - \widehat{\underline{F}}_E) + (\underline{W}_E - \widehat{\underline{W}}_E)\} \cdot \underline{F}^*_E \,\mathrm{d}\Gamma = \sum_{E\in\mathbf{E}} \int_{\partial\Omega_E} \widetilde{\underline{W}}^M_E \cdot \underline{F}^*_E \,\mathrm{d}\Gamma, \quad (10)$$

$$\forall \widetilde{\underline{W}}^{M*} \in \mathscr{W}^M_{\mathrm{ad},0}, \quad \sum_{E\in\mathbf{E}} \int_{\partial\Omega_E} \widetilde{\underline{W}}^{M*}_E \cdot \underline{F}_E \,\mathrm{d}\Gamma = \sum_{E\in\mathbf{E}} \int_{\partial\Omega_E\cap\partial_2\Omega} \widetilde{\underline{W}}^{M*}_E \cdot \underline{F}_d \,\mathrm{d}\Gamma. \quad (11)$$

Eq. (11) expresses the admissibility of the macroforces in a weak sense. The introduction of the two search directions (8) and (9) makes the problem well-posed. The problem can be split into two parts: a microproblem (see Section 3.3.1) defined over each substructure Ω_E and a global macroproblem defined over the whole set of interfaces (see Section 3.3.3). The macroproblem requires the definition of a homogenized behavior operator for each substructure Ω_E (Section 3.3.2). The definition of such an operator for a cracked substructure is discussed below.

3.3.1. The microproblem within a substructure Ω_E

The microproblem associated with Substructure Ω_E, $E \in \mathbf{E}$, is defined as follows:

Problem 2. Find $\mathbf{s}_E = (\varepsilon_E, \underline{W}_E, \sigma_E, \underline{F}_E) \in \mathbf{S}_E$ which verifies:
- the E-admissibility of s_E (see Definition 1),
- the search direction (10).

This is a linear problem. Since the search direction (10) is local over $\partial\Omega_E$, the microproblem consists in a set of independent problems within each substructure Ω_E. The kinematic admissibility equation (see Definition 1) and the linear constitutive law ($\sigma_E = \mathbf{K}{:}\varepsilon_E$) can be expressed in a weak sense as follows:

$$\forall (\sigma^*, \underline{F}^*) \in \mathbf{F}_{E,\mathrm{ad},0}, \quad \int_{\Omega_E} \sigma_E : \mathbf{K}^{-1} : \sigma^* \,\mathrm{d}\Omega = \int_{\partial\Omega_E} \underline{F}^* \cdot \underline{W}_E \,\mathrm{d}\Gamma. \quad (12)$$

Introducing the search direction (10) into (12), this leads to the following microproblem in terms of the stresses:

Problem 3. Find $(\sigma_E, \underline{F}_E) \in \mathbf{F}_{E,\mathrm{ad}}$ which verifies:

$$\forall (\sigma^*, \underline{F}^*) \in \mathbf{F}_{E,\mathrm{ad},0}, \quad \int_{\Omega_E} \sigma_E : \mathbf{K}^{-1} : \sigma^* \,\mathrm{d}\Omega + \int_{\partial\Omega_E} k^{-1}\underline{F}_E \cdot \underline{F}^* \,\mathrm{d}\Gamma = \int_{\partial\Omega_E} (k^{-1}\widehat{\underline{F}}_E + \widehat{\underline{W}}_E + \widetilde{\underline{W}}^M_E) \cdot \underline{F}^* \,\mathrm{d}\Gamma.$$

The microproblem over a substructure Ω_E can be reformulated in terms of the displacements:

Problem 4. Find $(\underline{u}_E, \underline{W}_E) \in \mathbf{E}_{E,\mathrm{ad}}$ which verify:

$$\forall (\underline{u}^*, \underline{W}^*) \in \mathbf{E}_{E,\mathrm{ad}}, \quad \int_{\Omega_E} \varepsilon(\underline{u}_E) : \mathbf{K} : \varepsilon(\underline{u}^*) \mathrm{d}\Omega + \int_{\partial\Omega_E} k\underline{W}_E \cdot \underline{W}^* \,\mathrm{d}\Gamma = \int_{\Omega_E} \underline{f}_{d|\Omega_E} \cdot \underline{u}^* \mathrm{d}\Omega + \int_{\partial\Omega_E} (\widehat{\underline{F}}_E + k\widehat{\underline{W}}_E + k\widetilde{\underline{W}}^M_E) \cdot \underline{W}^* \,\mathrm{d}\Gamma.$$

The solution of the microproblem associated with Substructure Ω_E depends only on the known quantities $\underline{f}_{d|\Omega_E}$, $\hat{\mathbf{s}}_E$ and $\widetilde{\underline{W}}^M_E$ over $\partial\Omega_E$ which is determined by the macroproblem (see Section 3.3.3). One can prove that:

Proposition 3. *If* $\mathbf{K}$ *and* k *are positive definite*, *Microproblem* (*Problem* 3) *defined over Substructure* Ω_E *and its boundary* $\partial\Omega_E$ *has a unique solution such that*:

$$\underline{F}^M_E = \mathbf{L}^F_E(\widetilde{\underline{W}}^M_E) + \widehat{\underline{F}}^M_{E,d}, \quad (13)$$

where $\widetilde{\underline{W}}^M_E \in \mathscr{W}^M_E = \prod_{E'\in\mathbf{V}_E} \mathscr{W}^M_{EE'}$ *and* $\widehat{\underline{F}}^M_{E,d}$ *depends on* $\underline{f}_{d|\Omega_E}$ *and* $\hat{s}_E$.

$\mathbf{L}^F_E$ is a linear operator from $\mathscr{W}^M_E$ onto $\mathscr{F}^M_E$ which can be interpreted as a homogenized behavior operator over substructure Ω_E. $\mathbf{L}^F_E$ is calculated by solving Microproblem for a set of loading cases $\widetilde{\underline{W}}^M_E$, with $\underline{f}_{d|\Omega_E}$ and $\hat{\mathbf{s}}_E$ set to zero. Note that $\widetilde{\underline{W}}^M_E$ depends on only a few scalar parameters: translations, rotations and extensions for a linear macrobasis (Fig. 3). Thus, the determination of $\mathbf{L}^F_E$ is obtained at relatively low cost. If n_M is the dimension of Space $\mathscr{W}^M_{EE'}$ for an interface $\Gamma_{EE'}$ and Ω_E is surrounded by n_i interfaces, then it takes $n_M \times n_i$ independent microproblems to determine $\mathbf{L}^F_E$. The properties of $\mathbf{L}^F_E$ are described in Section 3.3.2 below.

Let us recall that if one knows the Lagrange multiplier $\widetilde{\underline{W}}^M_E$, one can solve the microproblem over Ω_E and

determine $\mathbf{s}_E$ ($\hat{\mathbf{s}}_E$ being known from the previous local stage). Thus, there exists a localization operator $\mathbf{L}^s_E$ from $\mathscr{W}^M_E$ onto $\mathbf{S}_E$ such that:

$$\mathbf{s}_E = \mathbf{L}^s_E(\widetilde{W}^M_E) + \hat{\mathbf{s}}_{E,d},$$

where $\hat{\mathbf{s}}_{E,d}$ depends on $\hat{\mathbf{s}}_E$ and $\underline{f}_{d|\Omega_E}$.

3.3.2. The homogenized behavior operator for a substructure Ω_E

Let us first consider a crack-free structure Ω_E. During the linear stage, the force distribution $\underline{F}^M_E$ over $\partial\Omega_E$ is in equilibrium with the loading $\underline{f}_{d|\Omega_E}$ and belongs to the space:

$$\overline{\mathscr{F}}^M_{E,\mathrm{ad}} = \left\{ \underline{F}^M_E \in \mathscr{F}^M_E | \forall \underline{\alpha}_E \in \mathscr{R}_E, \int_{\partial\Omega_E} \underline{F}^M_E \cdot \underline{\alpha}_E \, \mathrm{d}\Gamma = \int_{\Omega_E} \underline{f}_d \cdot \underline{\alpha}_E \, \mathrm{d}\Omega \right\}, \tag{14}$$

where $\mathscr{R}_E = \{\underline{\alpha}_E \in \mathscr{U}_E | \varepsilon(\underline{\alpha}_E) = 0\}$ is the space of the infinitesimal rigid body modes of Ω_E. The corresponding vector space is denoted $\overline{\mathscr{F}}^M_{E,\mathrm{ad},0}$ (i.e. for $\underline{f}_d = 0$).

Proof 1. The solution of Microproblem (Problem 4) must verify:

$$\forall \underline{\alpha}_E \in \mathscr{R}_E, \quad \int_{\partial\Omega_E} \underline{F}_E \cdot \underline{\alpha}_E \, \mathrm{d}\Gamma = \int_{\Omega_E} \underline{f}_d \cdot \underline{\alpha}_E \, \mathrm{d}\Omega.$$

According to the definition of the macrodisplacement space, one has $\mathscr{R}^W_E \subset \mathscr{W}^M_E$, where $\mathscr{R}^W_E$ corresponds to the space which contains the trace on $\partial\Omega_E$ of each displacement field that belongs to $\mathscr{R}_E$. The uncoupling relation (6) between the micro work and the macro work enables one to write:

$$\forall \underline{\alpha}_E \in \mathscr{R}_E, \quad \int_{\partial\Omega_E} \underline{F}_E \cdot \underline{\alpha}_E \, \mathrm{d}\Gamma = \int_{\partial\Omega_E} \underline{F}^M_E \cdot \underline{\alpha}_E \, \mathrm{d}\Gamma.$$

Thus, $\underline{F}^M_E$ is in equilibrium with the loading $\underline{f}_{d|\Omega_E}$ and belongs to $\overline{\mathscr{F}}^M_{E,ad}$. □

Proposition 4. *Operator* $\mathbf{L}^F_E$

- *has its image in* $\overline{\mathscr{F}}^M_{E,\mathrm{ad},0}$,
- *is not definite and its kernel is* $\mathscr{R}^W_E$,
- *is a bijection from the quotient space* $\overline{\mathscr{W}}^M_E = \mathscr{W}^M_E / \mathscr{R}^W_E$ *onto* $\overline{\mathscr{F}}^M_{E,\mathrm{ad},0}$,
- *is positive for the work bilinear form* (1) *defined over* $\partial\Omega_E$.

Proof 2. Let us consider $\mathbf{s}_E = \mathbf{L}^s_E(\widetilde{W}^M_E)$ with $\hat{\mathbf{s}}_{E,d} = 0$. Thus, $\mathbf{s}_E$ belongs to $\mathbf{S}_{E,\mathrm{ad},0}$ and verifies the search direction (10):

$$\forall \underline{F}^* \in \mathscr{F}_E, \quad \int_{\partial\Omega_E} (k^{-1}\underline{F}_E + \underline{W}_E - \widetilde{W}^M_E) \cdot \underline{F}^* \, \mathrm{d}\Gamma = 0. \tag{15}$$

$\mathbf{s}_E$ is the solution of the following problem: Find $(\sigma_E, \underline{F}_E) \in \mathbf{F}_{E,h,\mathrm{ad}}$ such that:

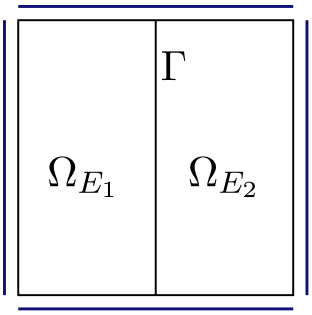

Fig. 9. A substructure Ω_E split into two parts Ω_{E_1} and Ω_{E_2} and surrounded by four interfaces.

$$\forall (\sigma^*, \underline{F}^*) \in \mathbf{F}_{E,\mathrm{ad},0}, \quad \int_{\Omega_E} \sigma_E : \mathbf{K}^{-1} : \sigma^* \, \mathrm{d}\Omega + \int_{\partial\Omega_E} k^{-1}\underline{F}_E \cdot \underline{F}^* \, \mathrm{d}\Gamma = \int_{\partial\Omega_E} \widetilde{W}^M_E \cdot \underline{F}^* \, \mathrm{d}\Gamma.$$

If one chooses $\mathbf{s}_E$ as a virtual field in this formulation, according to the uncoupling relation (6), one can write:

$$\int_{\partial\Omega_E} \widetilde{W}^M_E \cdot \underline{F}_E \, \mathrm{d}\Gamma = \int_{\partial\Omega_E} \widetilde{W}^M_E \cdot \mathbf{L}^F_E(\widetilde{W}^M_E) \mathrm{d}\Gamma.$$

Since $\mathbf{K}$ and k are positive definite operators, $\mathbf{L}^F_E$ is also positive. Moreover, if $\mathbf{L}^F_E(\widetilde{W}^M_E) = 0$, then $\sigma_E = 0$ and $\underline{F}_E = 0$. Using the constitutive law $\sigma_E = \mathbf{K}{:}\varepsilon_E$, one can say that $\varepsilon_E = 0$, which implies that $\underline{W}_E \in \mathscr{R}^W_E$. The search direction (15) yields $\underline{W}_E = \widetilde{W}^M_E$ and, consequently, $\widetilde{W}^M_E \in \mathscr{R}^W_E$. Thus, $Ker(\mathbf{L}^F_E) = \mathscr{R}^W_E$. Since $\mathbf{L}^F_E$ defines an injection from $\overline{\mathscr{W}}^M_E$ onto $\overline{\mathscr{F}}^M_{E,\mathrm{ad},0}$ (two spaces with the same finite dimension), $\mathbf{L}^F_E$ defines a bijection from $\overline{\mathscr{W}}^M_E$ onto $\overline{\mathscr{F}}^M_{E,\mathrm{ad},0}$. □

In the case of a substructure Ω_E which is split into two parts Ω_{E_1} and Ω_{E_2} by a traction-free crack Γ (Fig. 9), the properties of the homogenized operator $\mathbf{L}^F_E$ must be redefined. Let us introduce the following definition:

$$\mathscr{R}_E = \{(\underline{\alpha}_{E_1}, \underline{\alpha}_{E_2}) \in \mathscr{U}_{E_1} \times \mathscr{U}_{E_2} | \varepsilon(\underline{\alpha}_{E_1}) = 0, \varepsilon(\underline{\alpha}_{E_2}) = 0, \underline{\alpha}_{E_1} = \underline{\alpha}_{E_1} \text{ on } \Gamma\}.$$

This space $\mathscr{R}_E$ is similar to that introduced previously and contains the infinitesimal rigid body modes of Ω_{E_1} and Ω_{E_2} which are continuous over Γ. Let us define:

$$\widetilde{\mathscr{R}}_E = \{(\underline{\alpha}_{E_1}, \underline{\alpha}_{E_2}) \in \mathscr{U}_{E_1} \times \mathscr{U}_{E_2} | \varepsilon(\underline{\alpha}_{E_1}) = 0, \varepsilon(\underline{\alpha}_{E_2}) = 0\}$$

the space which contains the infinitesimal rigid body modes of Ω_{E_1} and Ω_{E_2}. $\mathscr{R}^W_E$ and $\widetilde{\mathscr{R}}^W_E$ are respectively the spaces of the traces of the functions of $\mathscr{R}_E$ and $\widetilde{\mathscr{R}}_E$ on $\partial\Omega_E$. The previous definitions of $\overline{\mathscr{F}}^M_{E,\mathrm{ad}}$ (Eq. (14)) and $\overline{\mathscr{F}}^M_{E,\mathrm{ad},0}$ with this new definition of $\mathscr{R}_E$ remain the same. Proposition 4 becomes:

Proposition 5. *For a substructure Ω_E split into two parts by a traction-free crack, operator* $\mathbf{L}^F_E$

- *has its image in* $\overline{\mathscr{F}}^M_{E,\mathrm{ad},0}$,
- *is not definite and its kernel is* $\widetilde{\mathscr{R}}^W_E \cap \mathscr{W}^M_E$,

- *is a bijection from the quotient space* $\overline{\mathscr{W}}_E^M = \mathscr{W}_E^M / \widetilde{\mathscr{R}}_E^W \cap \mathscr{W}_E^M$ *onto* $\overline{\mathscr{F}}_{E,\mathrm{ad},0}^M$,
- *is positive for the work bilinear form* (1) *defined over* $\partial\Omega_E$.

Proof 3. This proof is similar to Proof 2. The only difference is that the kernel of $\mathbf{L}_E^F$ reduces to $\widetilde{\mathscr{R}}_E^W \cap \mathscr{W}_E^M$. □

If one chooses linear or cubic continuous macrobases for the four interfaces, $\widetilde{\mathscr{R}}_E^W \cap \mathscr{W}_E^M$, the kernel of $\mathbf{L}_E^F$, reduces to $\mathscr{R}_E^W$. Fig. 10 illustrates the three resulting rigid body modes in the 2D case. If one chooses discontinuous macrobases for the two interfaces which are intersected by the crack, the kernel $\widetilde{\mathscr{R}}_E^W \cap \mathscr{W}_E^M$ of operator $\mathbf{L}_E^F$ reduces to $\widetilde{\mathscr{R}}_E^W$. Indeed, $\widetilde{\mathscr{R}}_E^W \subset \mathscr{W}_E^M$. Fig. 11 shows the six resulting rigid body modes in 2D. This result is essential in order to ensure the numerical scalability of the multiscale strategy applied to crack propagation.

In order to illustrate the numerical scalability of the approach, let us consider the example described in Fig. 12. The micromesh is shown in the upper left corner of Fig. 13. Three partitions into substructures and interfaces are proposed with 2×5, 4×10 and 8×20 substructures respectively. The crack was modeled using the X-FEM. The propagation aspect was not addressed. The integration of the X-FEM will be discussed in Section 4.

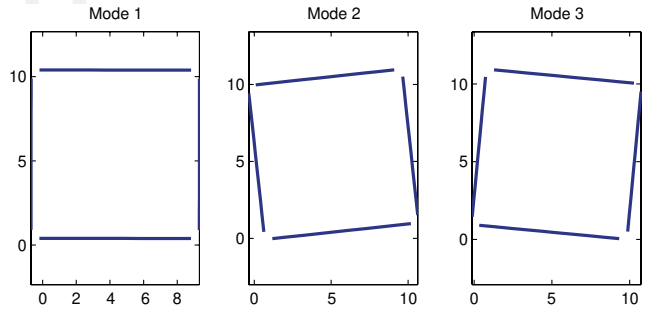

Fig. 10. With a linear or cubic continuous macrobasis for each interface, the kernel of operator $\mathbf{L}_E^F$ reduces to the rigid body modes (three modes in 2D) of the equivalent healthy substructure.

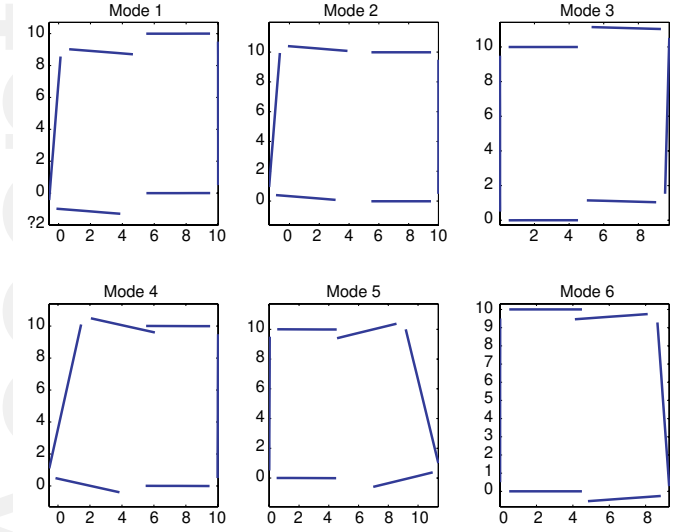

Fig. 11. For a discontinuous macrobasis, the kernel of operator $\mathbf{L}_E^F$ reduces to the rigid body modes (six modes in 2D) of the two parts Ω_{E_1} and Ω_{E_2} of Substructure Ω_E.

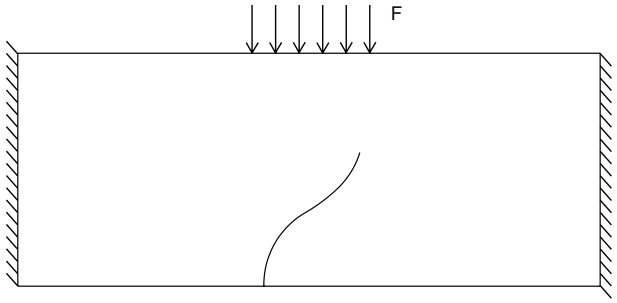

Fig. 12. Clamped structure with a traction-free crack subjected to bending.

The convergence curves of the LATIN error criterion η (16) for each partition and for the various macrobases (linear, cubic and discontinuous) are shown in Fig. 14. The convergence rate (i.e. the slope of the curves) with the discontinuous macrobasis is the same regardless of the partition. This is not the case of the linear and cubic continuous macrobases. Thus, it is necessary to introduce the discontinuity on the macroscale in order for the numerical scalability of the domain decomposition method to be unaffected by the presence of a crack.

3.3.3. The macroproblem over Ω

The macroproblem is defined by Eqs. (11) and (13). It can be expressed as follows:

Problem 5. Find $(\underline{\widetilde{W}}^M, \underline{F}^M)$ which verifies:

- kinematic admissibility: $\underline{\widetilde{W}}^M \in \mathscr{W}_{\mathrm{ad},0}^M$,
- static admissibility: $\underline{F}^M \in \mathscr{F}_{\mathrm{ad}}^M$,
- the homogenized constitutive law:

$$\forall E \in \mathbf{E}, \quad \underline{F}_E^M = \mathbf{L}_E^F(\underline{\widetilde{W}}_E^M) + \underline{\widehat{F}}_{E,d}^M.$$

The weak forms of the kinematic admissibility Eq. (11) and the constitutive law (13) lead to the following displacement formulation in terms of the multiplier $\underline{\widetilde{W}}^M$:

Problem 6. Find $\underline{\widetilde{W}}^M = \{\underline{\widetilde{W}}_E^M\}_{E\in\mathbf{E}} \in \mathscr{W}_{\mathrm{ad},0}^M$ which verifies:

$$\forall \underline{\widetilde{W}}^{M*} \in \mathscr{W}_{\mathrm{ad},0}^M, \quad \sum_{E\in\mathbf{E}} \int_{\partial\Omega_E} \underline{\widetilde{W}}_E^{M*} \cdot (\mathbf{L}_E^F(\underline{\widetilde{W}}_E^M) + \underline{\widehat{F}}_{E,d}^M)\,\mathrm{d}\Gamma = \sum_{E\in\mathbf{E}} \int_{\partial\Omega_E\cap\partial_2\Omega} \underline{\widetilde{W}}_E^{M*} \cdot \underline{F}_d\,\mathrm{d}\Gamma.$$

This problem has a unique solution if $mes(\partial_1\Omega) \neq 0$ [33].

Remark 4. Macroproblem (Problem 6) is solved exactly with no approximation. Consequently, the macroforce $(\underline{F}^M \in \mathscr{F}_{\mathrm{ad}}^M)$ and the multiplier $(\underline{\widetilde{W}}^M \in \mathscr{W}_{\mathrm{ad},0}^M)$ are admissible at each iteration. In the macroproblem is large, i.e. if it involves a large number of interfaces, it can be solved

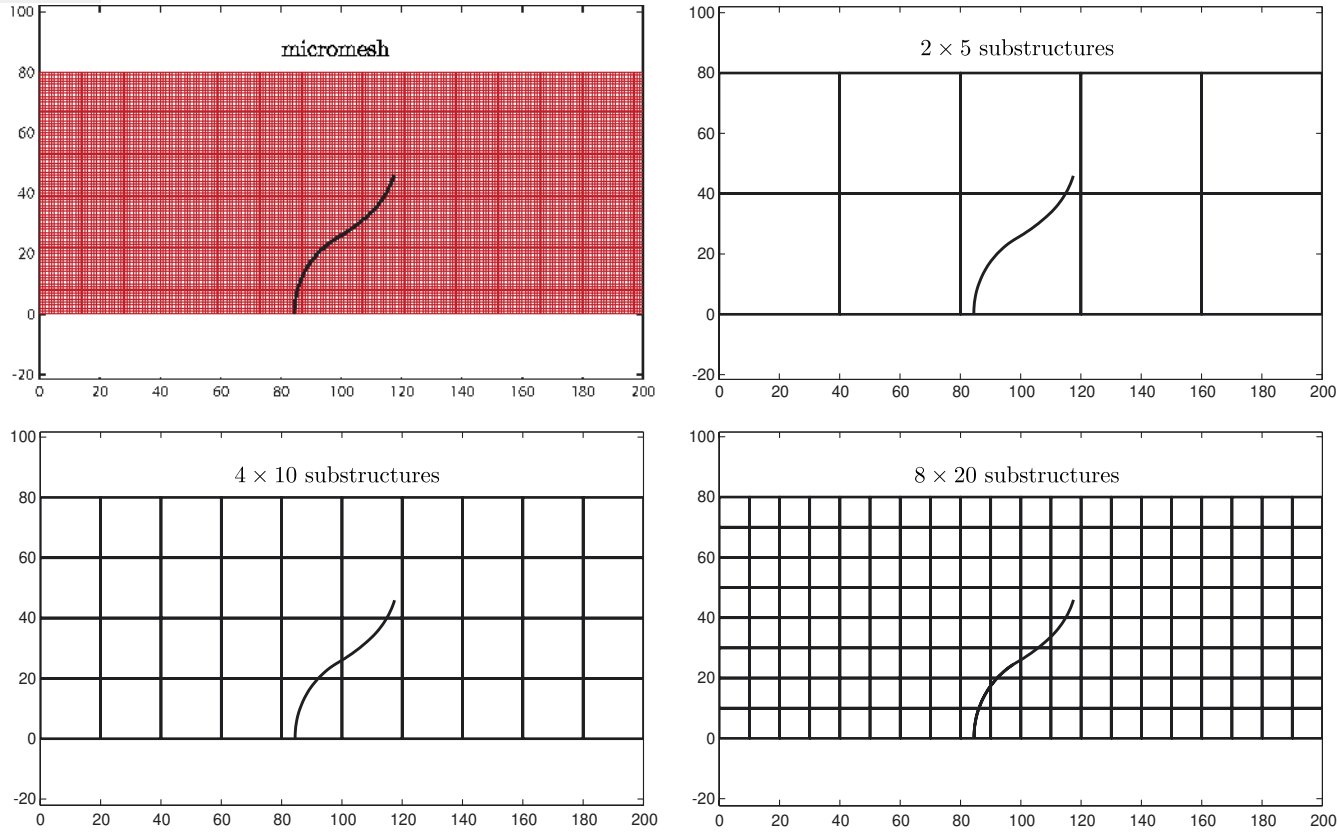

Fig. 13. The micromesh and three partitions into substructures and interfaces with 2×5, 4×10 and 8×20 substructures.

using an approximation of the multiplier ($\widetilde{\underline{W}}^M \in \mathcal{W}^M_{h,\mathrm{ad},0}$). This approximation space can be viewed as a third scale [20,33].

Remark 5. One can also use a formulation in terms of the macroforces [33]. Let us note that such a formulation introduces new unknowns: the traces of the rigid body modes of each substructure on the interfaces.

Remark 6. The macroquantities are defined only at the interfaces. The coupling between the microscale and the macroscale is achieved through the homogenized operator, which is nonlocal. Macroproblem (Problem 6) is not classical in that it does not involve a classical continuous medium. For a linear macrobasis, the kinematic unknowns $\{\widetilde{\underline{W}}^M_E\}_{E\in\mathbf{E}}$ correspond to translations, rotations and extensions at each interface. Such kinematics is comparable to that defined for a generalized Cosserat medium [35] or a micropolar medium [36].

3.4. Convergence of the strategy

If the material's behavior is monotonous and if the interfaces represent perfect links, boundary conditions or unilateral contact without friction, the multiscale strategy verifies the assumptions of the LATIN method [24]. If the search direction parameter k is positive, the convergence of the algorithm is guaranteed. Classically, for monoscale [37] and multiscale strategies based on the LATIN method, one uses an error indicator based on the conjugation of the search directions to control this convergence. For one iteration of the method, two consecutive solutions verify the search directions as follows:

$$(\widehat{\mathbf{s}}_{n+1/2} - \mathbf{s}_n) \in \mathbf{E}^+,$$
$$(\mathbf{s}_{n+1} - \widehat{\mathbf{s}}_{n+1/2}) \in \mathbf{E}^-.$$

The cross-verification of these two search directions means that the difference $\mathbf{s} - \widehat{\mathbf{s}}$ is zero in both cases and that convergence has been reached (Fig. 8). Thus, one defines the following error indicator:

$$\eta^2 = \frac{\sum_{E\in\mathbf{E}}[\|\underline{W}_E - \widehat{\underline{W}}_E\|^{W,k}_{\partial\Omega_E} + \|\underline{F}_E - \widehat{\underline{F}}_E\|^{F,k}_{\partial\Omega_E}]}{\sum_{E\in\mathbf{E}}[\|\underline{W}_E\|^{W,k}_{\partial\Omega_E} + \|\widehat{\underline{W}}_E\|^{W,k}_{\partial\Omega_E} + \|\underline{F}_E\|^{F,k}_{\partial\Omega_E} + \|\widehat{\underline{F}}_E\|^{F,k}_{\partial\Omega_E}]}, \tag{16}$$

where $\|\underline{W}\|^{W,k}_{\partial\Omega_E} = \int_{\partial\Omega_E} k\underline{W}\cdot\underline{W}\,\mathrm{d}\Gamma$ and $\|\underline{F}\|^{F,k}_{\partial\Omega_E} = \int_{\partial\Omega_E} \underline{F}\cdot k^{-1}\underline{F}\,\mathrm{d}\Gamma$.

In order to ensure convergence for many types of material behavior, the linear stage is modified in order to include a relaxation step [24]. After renaming $\mathbf{s}^{\sim}_{n+1}$, the previous quantity $\mathbf{s}_{n+1} \in \mathbf{A}_d$, $\mathbf{s}_{n+1}$ is now defined by:

$$\mathbf{s}_{n+1} = \mu\tilde{\mathbf{s}}_{n+1} + (1-\mu)\mathbf{s}_n,$$

where in practice, the relaxation parameter μ is equal to 0.8.

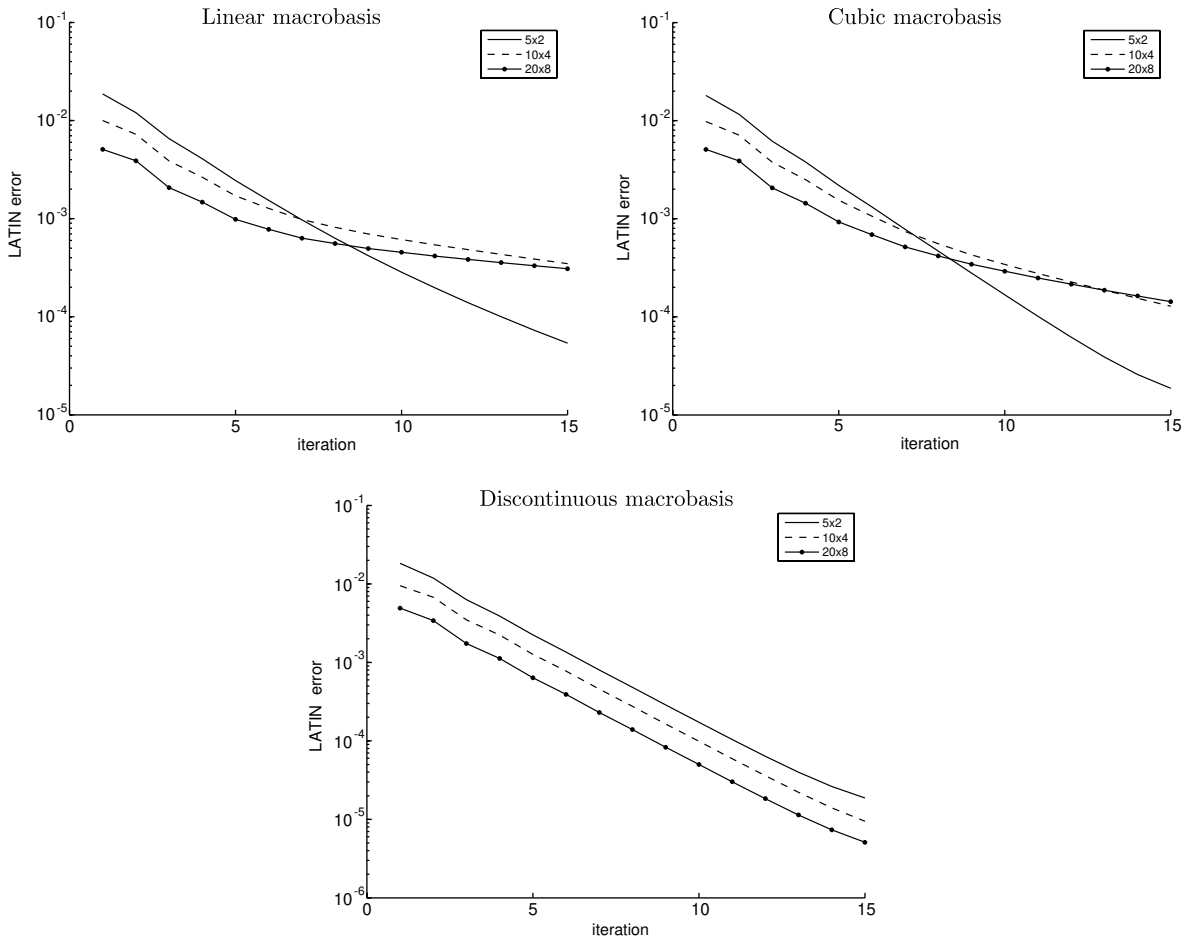

Fig. 14. LATIN error criterion η vs the number of iterations for different substructure partitions and macrobases.

3.5. The final algorithm

Microproblem (Problem 4) is solved using a finite element displacement formulation. The discretization of this problem leads to the following linear system:

$$([K_E] + [k_E])[\underline{u}_E] = [\widehat{\underline{F}}_{E,d}] + [k\widetilde{\underline{W}}_E^M]$$

where $[\cdot]$ represents the nodal values of the quantity being considered. $[K_E]$ is the stiffness matrix associated with Substructure E. $[k_E]$ is the interface stiffness matrix associated with the term $\int_{\partial\Omega_E} k\underline{W}_E \cdot \underline{W}^* \mathrm{d}\Gamma$. $[\widehat{\underline{F}}_{E,d}]$ is the loading vector corresponding to $\underline{f}_{d|\Omega_E}$ and $\hat{\mathbf{s}}_E$. Similarly, the discretization of Macroproblem (Problem 6) leads to the following linear system:

$$[\mathbf{L}^F]_{\mathbf{e}^M}[\widetilde{W}^M]_{\mathbf{e}^M} = [\widehat{\underline{F}}_d^M]_{\mathbf{e}^M} + [\underline{F}_d^M]_{\mathbf{e}^M}$$

where $[\cdot]_{\mathbf{e}^M}$ represents the components of the quantity being considered in the macrobasis. Macroproblem is a square system whose dimension is $\sum_{i=1\ldots n_\Gamma} n_M^{(i)}$, where $n_M^{(i)}$ is the number of macro unknowns (translations, rotations, extensions) for Interface i and n_Γ is equal to the number of interfaces. The vector $[\widehat{\underline{F}}_d^M]_{\mathbf{e}^M}$ is associated with the term $\sum_{E\in\mathbf{E}} \int_{\partial\Omega_E} \widetilde{\underline{W}}_E^{M*} \cdot \widehat{\underline{F}}_{E,d}^M \mathrm{d}\Gamma$ and $[\underline{F}_d^M]_{\mathbf{e}^M}$ corresponds to $\sum_{E\in\mathbf{E}} \int_{\partial\Omega_E\cap\partial_2\Omega} \widetilde{\underline{W}}_E^{M*} \cdot \underline{F}_d \mathrm{d}\Gamma$.

The initialization of the algorithm consists in finding a solution $\mathbf{s}_0$ which belongs to $\mathbf{A}_d$. First, one defines a solution $\hat{\mathbf{s}}_{-\frac{1}{2}}$ which verifies $\boldsymbol{\Gamma}$ by setting $\hat{\mathbf{s}}_{-\frac{1}{2}} \equiv 0$ and applying the boundary conditions to the corresponding "hat" interface quantities. Then, using the search direction $\mathbf{E}^-$, a first local stage leads to the solution $\mathbf{s}_0$ of $\mathbf{A}_d$. The main steps of the multiscale strategy are described below. Parallelizable steps are tagged with an empty square □.

(1) **Definition** of k and the macrobasis for each interface. In practice, $k = \alpha E/L$, where E is the Young's modulus, L a characteristic length of the interface and $\alpha = 10$. Note that an optimization loop for k could be introduced here.
(2) **Preliminary calculation:** For each substructure $E \in \mathbf{E}$:
   □ calculation of the stiffness matrices: $[K_E]$ and $[k_E]$
   □ assembly and factorization of $[K_E] + [k_E]$
   □ determination of the homogenized operator: $[\mathbf{L}_E^F]$
   and for the whole set of interfaces:
   □ assembly and factorization of $[\mathbf{L}^F]_{\mathbf{e}^M}$ for the macroproblem

(3) **Initialization:** $\mathbf{s}_0 \in \mathbf{A}_d$

(4) **LATIN loop:** For $n = 0$ to n_{max} do

(a) *Local stage*: calculation of $\widehat{\mathbf{s}}_{\mathbf{n+1/2}} \in \mathbf{\Gamma}$

☐ resolution of the local problem at each interface $\Gamma_{EE'}$

→ calculation of $(\widehat{\underline{F}}_{E,n+1/2}, \widehat{\underline{W}}_{E,n+1/2})$ and $(\widehat{\underline{F}}_{E',n+1/2}, \widehat{\underline{W}}_{E',n+1/2})$

(b) *Linear stage*: calculation of $\mathbf{s}_{n+1} \in \mathbf{A}_d$

☐ resolution of the microproblem for the known quantities $\hat{\mathbf{s}}_{E,n+1/2}$ and $\underline{f}_d$ in each substructure $E \in \mathbf{E}$: $([K_E] + [k_E])[\underline{\hat{u}}_E] = [\underline{\widehat{F}}_{E,d}]$

→ calculation of $\hat{\mathbf{s}}_{E,d,n+1} \Rightarrow \underline{\widehat{F}}^M_{E,d,n+1}$

☐ resolution of the macroproblem

→ calculation of $\underline{\widetilde{W}}^M_{n+1}$

☐ resolution of the microproblem for the loading $\underline{\widetilde{W}}^M_{E,n+1}$ in each substructure $E \in \mathbf{E}$: $([K_E] + [k_E])[\underline{\tilde{u}}_E] = [k\underline{\widetilde{W}}^M_E]$

→ calculation of $\underline{u}_E = \underline{\hat{u}}_E + \underline{\tilde{u}}_E \Rightarrow \mathbf{s}_{E,n+1}$

☐ relaxation

→ $\mathbf{s}_{n+1} \rightarrow \tilde{\mathbf{s}}_{n+1}$,

→ $\mathbf{s}_{n+1} = \mu\tilde{\mathbf{s}}_{n+1} + (1-\mu)\mathbf{s}_n$ where $\mu = 0.8$ in practice

(c) Convergence criterion η

End LATIN loop

Remark 7. Aside from the macroproblem, in the particular case of perfect connections and linear elasticity, such an algorithm is similar to that based on the extension of the Schwartz algorithm to a non-overlapping domain decomposition method using an augmented Lagrangian formulation [38]. More precisely, the resulting algorithm corresponds to a Uzawa algorithm for the resolution of saddle-point problems, called ALG3 in [38].

4. Integration of the X-FEM on the microscale

4.1. Approximation space in a cracked substructure

In Section 2, we proposed a separation of the macroscale and microscale in order to take into account the effect of a crack on both the global and local levels. A discontinuous macrobasis was introduced. Such an enriched macrobasis enables one to keep a macromesh unchanged regardless of the crack's configuration, which eliminates the meshing difficulties on the macrolevel. In order to overcome the same difficulties on the microlevel, the X-FEM can be used as a tool to describe the crack in the zone of interest.

Since the scale separation is introduced only at the interfaces (see Section 2.2), Microproblem (Problem 4) on a substructure Ω_E is a classical problem in terms of displacement $\underline{u}_E$ with Robin conditions (search direction (10)). In a finite element displacement formulation of this problem,

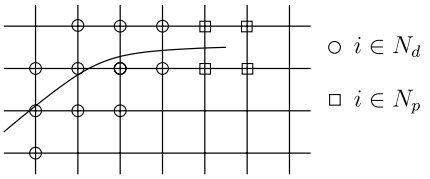

Fig. 15. Enriched nodes for the representation of a crack with a uniform mesh. The nodes surrounded by a circle are enriched with the discontinuity. The nodes surrounded by a square are enriched with the set of branch functions $\{F_j\}$.

nothing precludes the enrichment of the approximation of the displacement field in a substructure according to the X-FEM [27]. We propose to use a classical X-FEM approximation for $\underline{u}_E$ as described in [10,13]:

$$\forall \underline{x} \in \Omega_E, \quad \underline{u}_{E_h}(\underline{x}) = \sum_{i \in N} \varphi_i(\underline{x})\underline{u}_i + \sum_{i \in N_d} \varphi_i(\underline{x})H(\underline{x})\underline{a}_i + \sum_{i \in N_p} \varphi_i(\underline{x}) \sum_{j=1}^{4} F_j(\underline{x})\underline{b}_i^j \Bigg), \tag{17}$$

where H is the discontinuous function and $\{F_j\}$ are the branch functions (Fig. 15).

4.2. The approximation space at a cracked interface

Let us consider an interface $\Gamma_{EE'}$ between two substructures Ω_E and $\Omega_{E'}$. The macrobasis is defined prior to any discretization. Therefore, the definitions of the macro- and microquantities (Definition 2) are unchanged. The difficulty consists in expressing the kinematic admissibility of the displacement field $\underline{u}_E$ (respectively $\underline{u}_{E'}$) at the edge of a substructure Ω_E (respectively $\Omega_{E'}$) and the interface displacement $\underline{W}_E$ (respectively $\underline{W}_{E'}$). Thus, for the interface $\Gamma_{EE'}$:

$$\forall \underline{F}^* \in \mathscr{F}_{EE'}, \quad \int_{\Gamma_{EE'}} \underline{F}^* \cdot (\underline{u}_E - \underline{W}_E) \mathrm{d}\Gamma = 0. \tag{18}$$

The interface quantities for an interface intersected by a crack can also be enriched using for a displacement quantity the discontinuous H function as follows:

$$\underline{W} = \sum_{i \in N_\Gamma} \psi_i(\underline{x})\underline{w}_i + \sum_{i \in N_{\Gamma_d}} \psi_i(\underline{x})H(\underline{x})\underline{a}_{\Gamma_i}. \tag{19}$$

The same approximation can be used for a force quantity $\underline{F}$. After discretization, (18) leads to the system:

$$[N_{EE'}][B_{EE'}][d_E] = [M_{EE'}][W_E], \tag{20}$$

where $[B_{EE'}]$ is a Boolean operator which restricts the vector of the nodal unknowns $[d_E]$ of the displacement $\underline{u}_E$ to the edge $\Gamma_{EE'}$. $[d_E]$ contains the classical degrees of freedom $\underline{u}_i$ as well as the enriched degrees of freedom $\underline{a}_i$ and $\underline{b}_i$. $[W_E]$ is the vector of the nodal unknowns of the interface displacement $\underline{W}_E$ along $\Gamma_{EE'}$ and contains both the classical degrees of freedom $\underline{w}_i$ and the enriched degrees of freedom

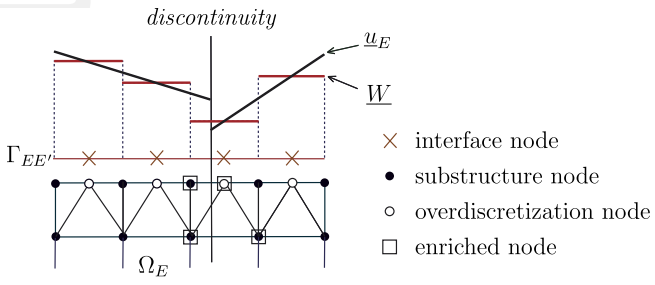

Fig. 16. Approximation space for an interface quantity $\underline{W}$ at an interface $\Gamma_{EE'}$ intersected by a crack: piecewise constant P0 shape functions.

$\underline{a}_{\Gamma_i}$. For the matrices $[N_{EE'}]_{ij} = (\tilde{\psi}_i, \tilde{\varphi}_{j|\Gamma_{EE'}})_{\Gamma_{EE'}}$ and $[M_{EE'}]_{ij} = (\tilde{\psi}_i, \tilde{\psi}_{j|\Gamma_{EE'}})_{\Gamma_{EE'}}$, $\tilde{\varphi}_i$ (respectively $\tilde{\psi}_i$) represent without distinction the classical finite element shape functions φ_i (respectively ψ_i) of a classical degree of freedom and the enriched shape functions $H\varphi_i$ (respectively $H\psi_i$) and $F_j\varphi_i$ of an enriched degree of freedom.

Another possibility consists in choosing for ψ_i piecewise constant functions. This choice is inspired by the discussion of the choice of the approximation spaces $\mathscr{F}_{EE',h}$ and $\mathscr{W}_{EE',h}$ in Section 2.1. This approximation space enables one to represent a discontinuity in a natural manner without introducing the discontinuous H function. Thus, one has simply:

$$\underline{W} = \sum_{i \in N_\Gamma} \psi_i(\underline{x}) \underline{w}_i \quad \text{and} \quad \underline{F} = \sum_{i \in N_\Gamma} \psi_i(\underline{x}) \underline{f}_i. \tag{21}$$

From here on, we will use piecewise constant P0 functions for all interface quantities at an interface intersected by a discontinuity (Fig. 16). Overdiscretization will be applied at the edges of the substructures in order to avoid spurious oscillating interforces as described in Section 2.1.

Remark 8. The discretization of an interface quantity (21) leads only to an approximate location of the discontinuity. A discontinuity is described properly only when the crack's path is aligned with the edges of the interface elements. Obviously, an enrichment using the jump function H, as in (19), is preferable. Such discretization is currently being studied.

4.3. Cracked plate under three-point bending

In order to illustrate the combined use of the X-FEM and the micro–macro approach, a cracked plate under three-point bending (Fig. 17) was studied. The propagation aspect was not addressed. Only two substructures were refined (Fig. 18). In [25,26], a new interface behavior was proposed for each interface between a refined substructure in the crack's vicinity and a coarse substructure. For a nonconforming interface $\Gamma_{EE'}$ between two nonconforming substructures Ω_E and $\Omega_{E'}$, relation (3) is:

$$\begin{cases} \underline{F}_E^M + \underline{F}_{E'}^M = 0 \\ \underline{W}_E^M - \underline{W}_{E'}^M = 0 \end{cases} \quad \text{and} \quad \begin{cases} \underline{F}_E^m = 0 \\ \underline{F}_{E'}^m = 0 \end{cases} \quad \forall \underline{x} \in \Gamma_{EE'}$$

This link, which forces the microforces to be equal to zero, ensures the transmission of forces and moments at the boundary of the refined zone and leads to a solution with minimal errors in the zone of interest. In our case, such a link with $\underline{F}^m = 0$ was used for the five interfaces

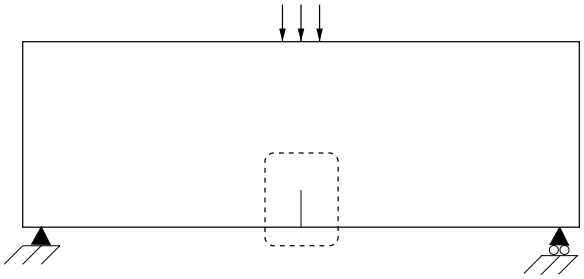

Fig. 17. Short plate with a single-edge crack under three-point bending.

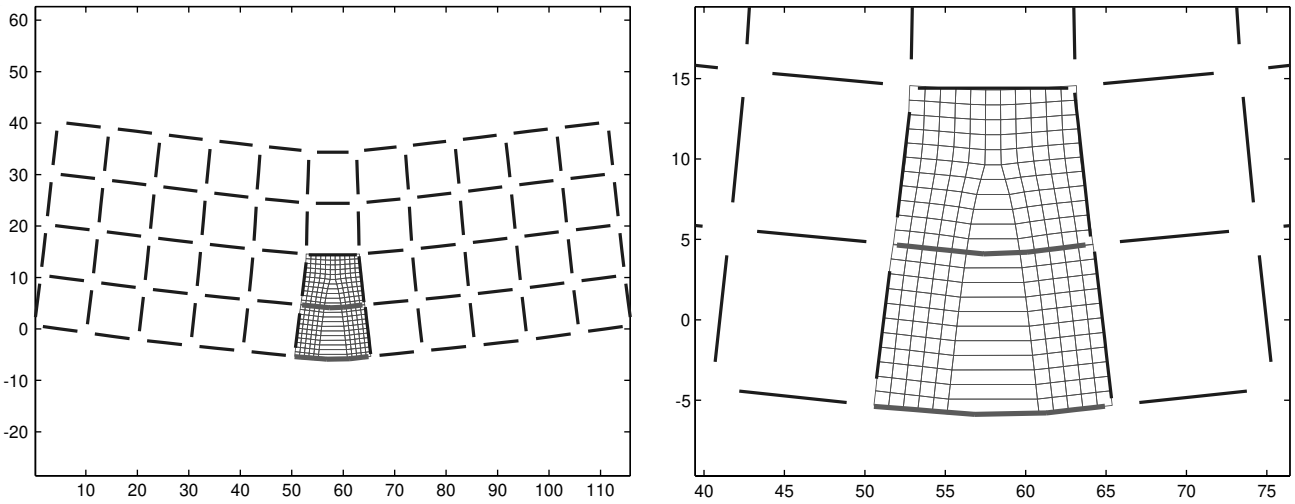

Fig. 18. Micro deformed shape in the cracked zone and interface macrodisplacement $\underline{W}^M$ (thick lines). A discontinuous macrobasis was defined for the two interfaces intersected by the crack and the X-FEM was used on the microlevel.

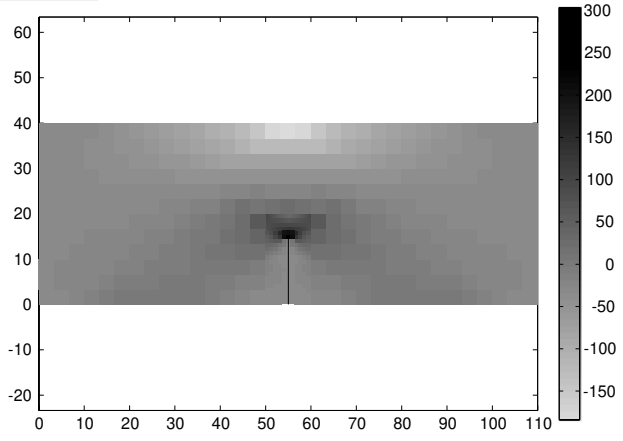

Fig. 19. Cracked plate under three-point bending: stress σ_{xx} (the x-axis is horizontal).

surrounding the refined substructures. A discontinuous macrobasis and a perfect link were used for the two interfaces located within the cracked zone.

The resulting deformed shape and interface macrodisplacement $\underline{W}^M$ (thick lines) are shown in Fig. 18. One can see that the macrodisplacement is discontinuous for the two interfaces intersected by the crack (see the zoom in Fig. 18). One should note that for the sake of simplicity the displacement within the substructures is interpolated over the geometry and not over the X-FEM shape functions. This explains why the elements intersected by the crack are stretched. The stress σ_{xx} is shown in Fig. 19. One can see that the X-FEM enabled the description of the singularity at the crack's tip even though a very coarse mesh was being used. The calculated value of the stress intensity factor K_I is $K_I = 665.23\ \text{MPa}\sqrt{\text{mm}}$. This agrees well with the reference value obtained by Gettu, Bažant and Karr [39]: $K_{I\text{ref}} = 664.69\ \text{MPa}\sqrt{\text{mm}}$. The relative error is about 0.08%.

5. The MS-X-FEM for fatigue crack propagation

5.1. Crack propagation with level set functions

A single level set function φ is sufficient to model a curve [30,31]. In order to model a crack in 2D, two level set functions are required (Fig. 20): one for the crack's faces (φ) and one to describe the crack's front (ψ). Provided that an initial description of the discontinuity Γ (e.g. a straight precrack defined by a line in 2D as in Fig. 20) is available at t_0, the level set functions $\varphi(\underline{x},t_0)$ and $\psi(\underline{x},t_0)$ can be expressed as follows:

$$\varphi(\underline{x},t_0) = \pm \min_{\underline{x}_\Gamma \in \Gamma(t_0)} \|\underline{x} - \underline{x}_\Gamma\|,$$

$$\psi(\underline{x},t_0) = (\underline{x} - \underline{x}_{pf}).\underline{t}_0.$$

Subsequently, an evolution equation [30] is used to update the level set functions. Thus, at a given time t, the crack's

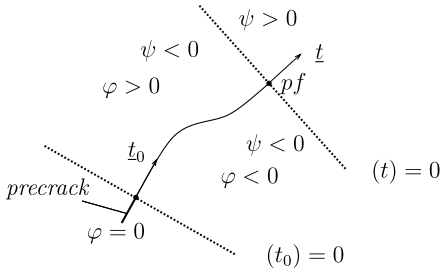

Fig. 20. Modeling of a crack with two level set functions: φ to model the crack's faces and ψ to locate the crack's tip pf.

position $\Gamma(t)$ can be expressed as a function of the updated values of φ and ψ:

$$\Gamma(t) := \{\underline{x} \in \mathbb{R}^2 | \varphi(\underline{x},t) = 0 \text{ and } \psi(\underline{x},t) \leqslant 0\}.$$

Once the level set functions φ, ψ are known, the enrichment functions $H(\underline{x})$ and $\{F_l(r,\theta)\}$ can be easily evaluated using the following expressions given in [13]:

$$H(\underline{x},t) = H^*(\varphi(\underline{x},t)) = \begin{cases} 1 & \text{for} \quad \varphi(\underline{x},t) > 0, \\ -1 & \text{for} \quad \varphi(\underline{x},t) < 0 \end{cases}$$

and

$$r = \sqrt{\varphi^2(\underline{x},t) + \psi^2(\underline{x},t)},$$

$$\theta = \arctan \frac{\varphi(\underline{x},t)}{\psi(\underline{x},t)}.$$

The level set functions are also used to identify the interfaces which are intersected by the crack and the location of the cut along these cut interfaces. Then, the corresponding discontinuous macrobasis (Fig. 4) can be defined. The crack's propagation is achieved by updating the level set functions and the values of the enrichment functions. For a 2D problem, the algorithm used to update the level set functions is described in [13].

5.2. MS-X-FEM algorithm for fatigue crack propagation

In this section, we present the MS-X-FEM algorithm for fatigue crack propagation. The propagation law is determined explicitly using the Paris law and the maximum hoop stress criterion. In this case, the problem corresponds to the resolution of a static problem at each propagation step. A crack length increment control is chosen. For each crack length step, the problem is solved by the micro–macro approach (see the algorithm in Section 3.5) using an X-FEM model of the current position of the crack. The resulting algorithm can be written as follows:

(1) **Definition** of pre-crack geometry, crack length increment Δa and list of the refined substructures $\mathbf{E}_f^{(0)}$ at Step (0).
(2) **Preliminary calculation at Step (0):**
   □ For each substructure of $\mathbf{E}_f^{(0)}$:
   → initialization of the level set functions,

→ enrichment: X-FEM + discontinuous macrobasis,

☐ For each substructure of **E**:

→ calculation and factorization of the stiffness matrices,

→ determination of the homogenized operator $[\mathbf{L}_E^F]$.

☐ Assembly and factorization of $[\mathbf{L}^F]_{\mathbf{e}^M}^{(0)}$ for the macroproblem.

(3) **Propagation loop:** For $p = 1$ to n_{step} do

(a) *Initialization:* $\mathbf{s}_0^{(p)} \in \mathbf{A}_d$

(b) *LATIN loop*: convergence criterion $\eta < 10^{-4}$ (heuristic criterion)

(c) *SIF calculation*: calculation of the branching angle, propagation of the crack

(d) *Updating stage at Step (p)*:

→ updating of $\mathbf{E}_f^{(p)} \to \mathbf{E}_f^{(p+1)}$,

→ for each substructure of $\mathbf{E}_f^{(p+1)}$: updating of the level sets, enrichment functions, macrobasis and homogenized operator $[\mathbf{L}_E^F]$,

→ assembly and factorization of $[\mathbf{L}^F]_{\mathbf{e}^M}^{(p+1)}$

End propagation loop

Remark 9. Note that the updating stage is performed only for the refined substructures. Let us recall that the link with $\underline{F}^n = 0$ which is used for the interfaces between refined substructures and coarse substructures connects only the macroforce and macrodisplacement components, regardless of the discretization. Consequently, this updating process does not affect the homogenized operators of the coarse substructures.

Remark 10. Updating the list of the refined substructures requires the definition of an error estimator in order to define the size of the zone where a fine description is needed. This question is not addressed in this paper.

5.3. Fatigue crack propagation in a plate with three holes

Let us consider the fatigue propagation of a precrack in a plate with three holes under three-point bending (Fig. 21). This case was studied in [40]. Plane strain and linear elastic material are assumed. The Young's modulus and Poisson's ratio are set to $E = 200{,}000$ MPa and $\nu = 0.3$. The Paris law was used and the propagation direction was determined using the maximum hoop stress criterion (even though this criterion can be questioned when the crack's tip interacts with a hole). A crack length increment control was chosen and the propagation increment was set to $\Delta a = 0.1$ mm. The macromesh of the interfaces and the micromesh within the refined substructures for the MS-X-FEM are shown in Fig. 22. For the sake of simplicity, the micromesh was defined *a priori* in the zone where the crack propagates. The link with $\underline{F}^n = 0$ was used for the interfaces surrounding the refined substructures. Moreover, in order to study the effect of the choice of the macrobasis, linear, cubic and discontinuous macrobases (Figs. 6 and 7) were tested successively for the interfaces located within the refined zone. We will use the direct X-FEM calculation as the reference. The reference mesh is shown in Fig. 23. One should note that in the refined zone the reference mesh is similar to the MS-X-FEM mesh (Fig. 22).

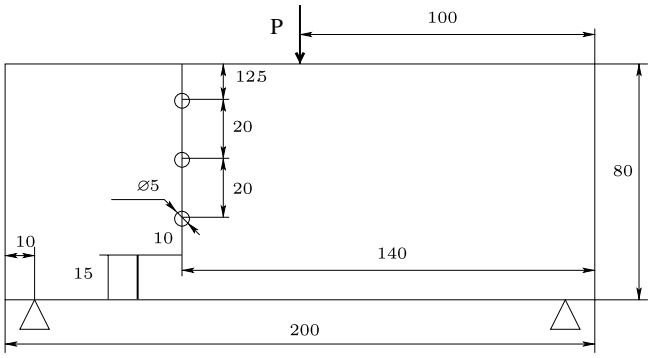

Fig. 21. Plate with a crack and three holes under three-point bending.

The resulting crack's paths for the MS-X-FEM with different macrobases and for the direct X-FEM calculation are shown in Fig. 24. The results are very similar to the crack's path obtained with the direct X-FEM calculation, especially in the case of the discontinuous macrobasis. Nevertheless, for the other macrobases, some deflections of the crack's path can be observed during the propagation. Indeed, while the heuristic convergence criterion, which was set to $\eta = 10^{-4}$ (see the algorithm in Section 5.2), seems to be sufficient for the discontinuous macrobasis, the solution at each propagation step is not sufficiently accurate for the linear and cubic macrobases. Therefore, the calculated stress intensity factor is erroneous and diverges (Fig. 24). One should note that with the discontinuous macrobasis the convergence criterion $\eta = 10^{-4}$ leads to less than 1% error in *KI* throughout the computation.

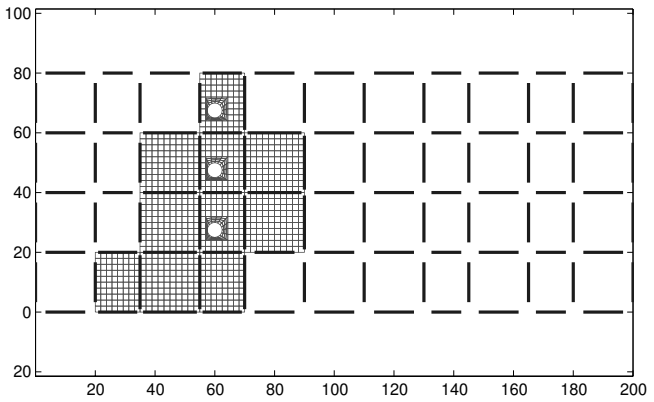

Fig. 22. Micromesh within the refined substructures and macromesh of the interfaces.

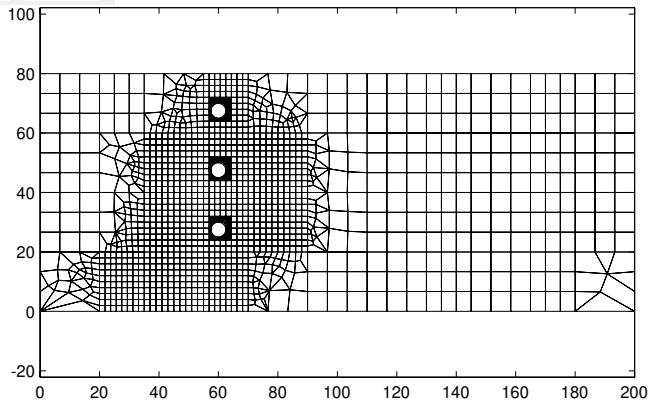

Fig. 23. X-FEM mesh used for the direct calculation (reference).

The deformed shapes with the X-FEM and the MS-X-FEM calculations are presented in Fig. 25 and the upper left corner of Fig. 26 respectively.

More precisely, the displacements within the refined substructures and the macrodisplacements $\underline{W}^M$ at the interfaces obtained with the different macrobases are shown in Fig. 26. All the deformed shapes are very similar. One can observe that the discontinuous macrobasis leads to interface macrodisplacements $\underline{W}^M$ very close to the total interface displacement $\underline{W}$. The complementary part $\underline{W}^m$ is nearly zero. The homogenized operator is definitely capable of representing the separation of the two parts of each substructure intersected by the crack (see Proof 3 in Section 3.3.2).

The number of LATIN iterations required at each propagation step for the different macrobases with the convergence criterion set to $\eta = 10^{-4}$ is shown in Fig. 27. The use of a discontinuous macrobasis leads to a number of iterations equal to about 10 and quasi-constant throughout the propagation. Conversely, for the linear and the cubic macrobases, this number keeps increasing drastically. Our interpretation is that the macroproblem which results from the use of a discontinuous macrobasis is capable of representing the macroeffect of the crack regardless of its geometry and achieves proper scale separation. Let us recall that only the discontinuous macrobasis can represent the rigid body modes of a substructure split by a crack (see Section 3.3.2). Indeed, the interface macroforces are sufficient to recover the interior solution within all substructures, even though one substructure contains the crack. The effect of the interface microforces is localized only in the vicinity of each interface. This is not the case with the linear and cubic macrobases, where the microquantities are essential to represent the global effect of the crack.

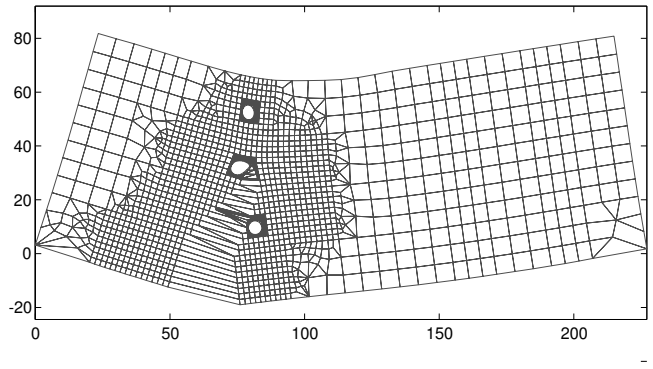

Fig. 25. Deformed shape with the direct X-FEM calculation in the last propagation step.

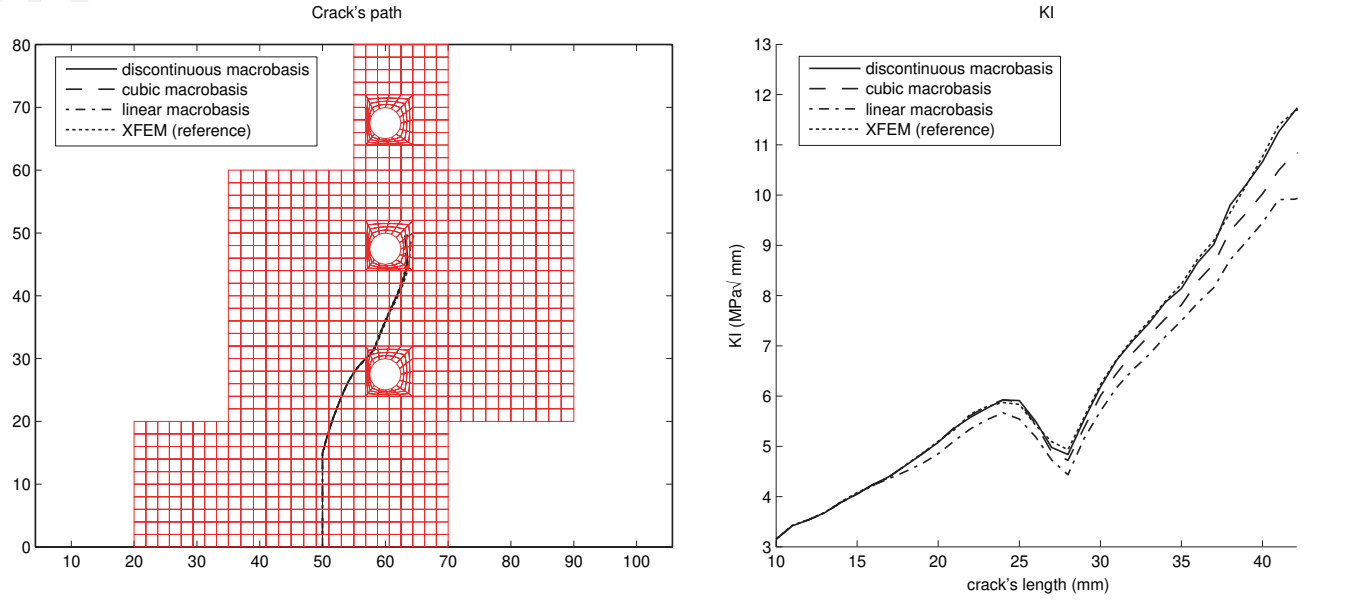

Fig. 24. Crack's paths for the MS-X-FEM and values of *KI* as a function of the crack's length for different macrobases and for the direct X-FEM computation (reference).

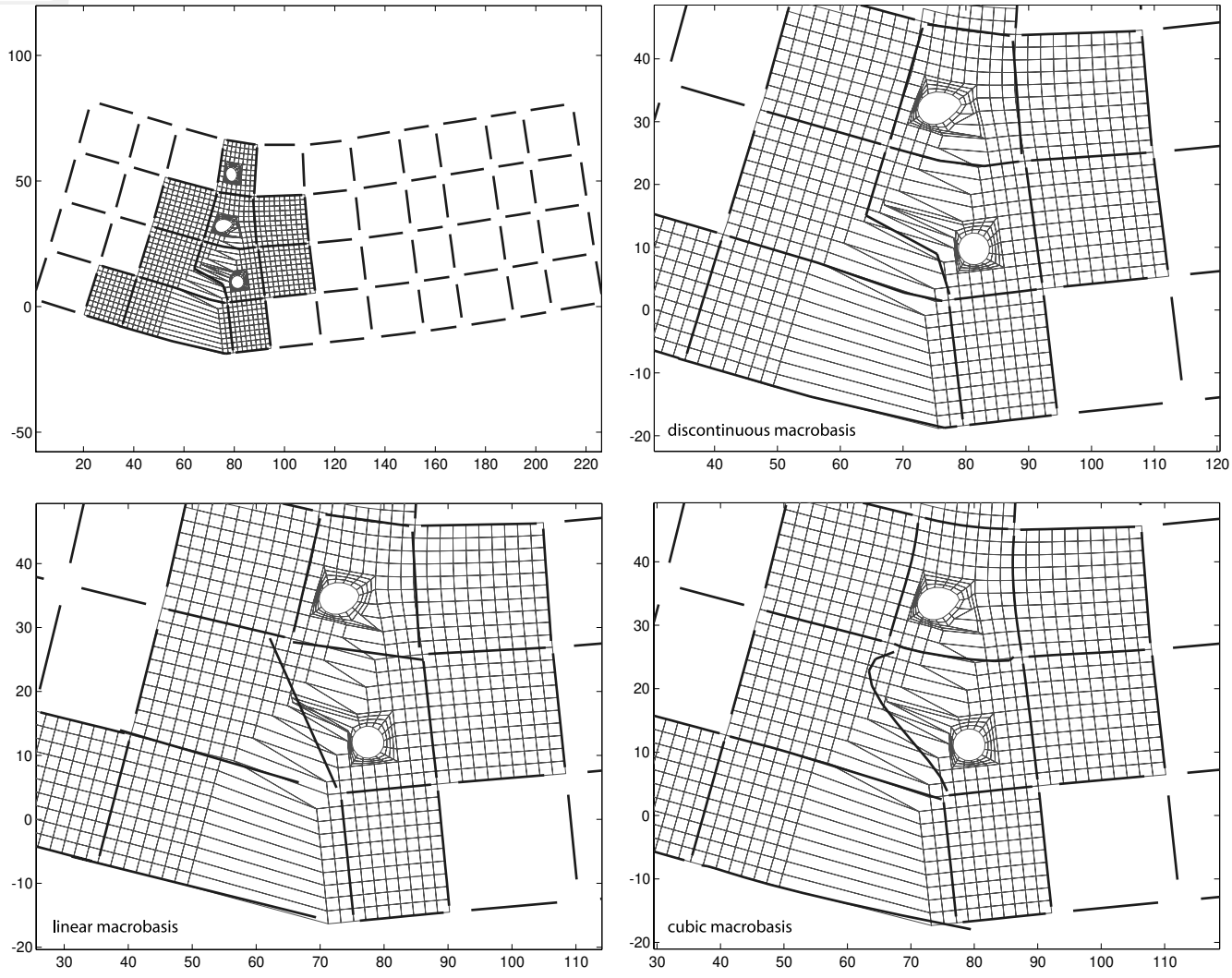

Fig. 26. Deformed shape in the refined substructures and macrodisplacements $\underline{W}^M$ at the interfaces (thick lines) obtained with linear, cubic and discontinuous macrobases.

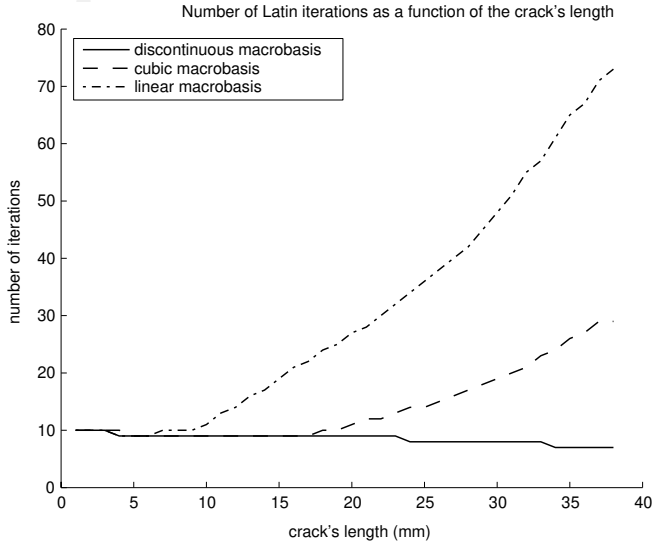

Fig. 27. Number of LATIN iterations as a function of the crack's length for the different macrobases with the convergence criterion set to $\eta = 10^{-4}$.

6. Conclusion

In this paper, we presented a multiscale strategy for crack propagation called the MS-X-FEM. This strategy puts two techniques into synergy: a micro–macro approach for the efficient treatment of the global and local effects due to the crack, and a local enrichment technique, the X-FEM, for the description of the geometry of the crack independently of the mesh.

The first motivation of this work was to develop a strategy which makes remeshing unnecessary during a crack's propagation. The micro–macro approach, based on a mixed domain decomposition method, enables one to use a refined mesh only in the vicinity of the crack and independently of the coarse mesh, so that the element's size is sufficient to get an accurate solution when the crack modeled by the X-FEM interacts with the coarse scale. Similar to the X-FEM on the microscale, the remeshing process consists in using an enriched macrobasis and adding new

macro unknowns. Therefore, both the macromesh of the interfaces and the micromesh are unchanged.

Another point concerns the definition of scales. Since a crack affects both the local and global responses of the structure, a suitable scale separation was required in order for the strategy to be efficient. We showed that the introduction of the crack's discontinuity both on the microscale and on the macroscale is advisable and does not deteriorate the convergence rate of the iterative solver when the crack propagates. In this case, the homogenized operator of a subdomain intersected by a crack can represent the rigid body modes of each part resulting from the separation, which is essential in order to guarantee the numerical scalability of the multiscale strategy.

Even though the algorithm of the MS-X-FEM was presented in the context of fatigue crack propagation with traction-free cracks, nothing prevents the application of this strategy to other types of propagation problems. Currently, we are working on the propagation of cracks with frictional contact. Another pending issue is the definition of an error estimator to control the size of the refined zone around the crack's tip.

References

[1] I. Hirai, B.P. Wang, W.D. Pilkey, An efficient zooming method for finite element analysis, Int. J. Numer. Methods Engrg. 20 (1984) 1671–1683.

[2] I. Hirai, Y. Uchiyama, Y. Mizuta, W.D. Pilkey, An exact zooming method, Finite Elements Anal. Des. 1 (1985) 61–69.

[3] K.M. Mao, C.T. Sun, A refined global–local finite element analysis method, Int. J. Numer. Methods Engrg. 32 (1991) 29–43.

[4] J.D. Whitcomb, Iterative global/local finite element analysis, Comput. Struct. 40 (1991) 1027–1031.

[5] J. Oliver, On the discrete constitutive models induced by strong discontinuity kinematics and continuum constitutive equations, Int. J. Solids Struct. 37 (2000) 7207–7229.

[6] J. Oliver, A.E. Huespe, M.D.G. Pulido, E. Chaves, From continuum mechanics to fracture mechanics: the strong discontinuity approach, Engrg. Fract. Mech. 69 (2002) 113–136.

[7] J. Oliver, A.E. Huespe, M.D.G. Pulido, E. Samaniego, On the strong discontinuity approach in finite deformation settings, Int. J. Numer. Methods Engrg. 56 (2003) 1051–1082.

[8] J.M. Melenk, I. Babuška, The partition of unity finite element method: basic theory and applications, Comput. Methods Appl. Mech. Engrg. 139 (1996) 289–314.

[9] T. Belytschko, T. Black, Elastic crack growth in finite elements with minimal remeshing, Int. J. Numer. Methods Engrg. 45 (5) (1999) 601–620.

[10] N. Moës, J. Dolbow, T. Belytschko, A finite element method for crack growth without remeshing, Int. J. Numer. Methods Engrg. 46 (1999) 131–150.

[11] J. Dolbow, N. Moës, T. Belytschko, Discontinuous enrichment in finite elements with a partition of unity method, Finite Elements Anal. Des. 36 (2000) 235–260.

[12] C. Daux, N. Moës, J. Dolbow, N. Sukumar, T. Belytschko, Arbitrary branched and intersecting cracks with the extended finite element method, Int. J. Numer. Methods Engrg. 48 (2000) 1741–1760.

[13] M. Stolarska, D.L. Chopp, N. Moës, T. Belytschko, Modelling crack growth by level sets and the extended finite element method, Int. J. Numer. Methods Engrg. 51 (8) (2001) 943–960.

[14] N. Moës, A. Gravouil, T. Belytschko, Non-planar 3D crack growth by the extended finite element and level sets – Part I: Mechanical model, Int. J. Numer. Methods Engrg. 53 (2002) 2549–2568.

[15] N. Moës, A. Gravouil, T. Belytschko, Non-planar 3D crack growth by the extended finite element and level sets – Part II: Level set update, Int. J. Numer. Methods Engrg. 53 (2002) 2569–2586.

[16] T. Strouboulis, I. Babuška, K. Copps, The design and analysis of the Generalized Finite Element Method, Comput. Methods Appl. Mech. Engrg. 181 (2000) 43–69.

[17] T. Strouboulis, K. Copps, I. Babuška, The generalized finite element method, Comput. Methods Appl. Mech. Engrg. 190 (2001) 4081–4193.

[18] P. Ladevèze, D. Dureisseix, A micro/macro approach for parallel computing of heterogeneous structures, Int. J. Comput. Civil Struct. Engrg. 1 (2000) 18–28.

[19] P. Ladevèze, O. Loiseau, D. Dureisseix, A micro–macro and parallel computational strategy for highly heterogeneous structures, Int. J. Numer. Methods Engrg. 52 (1–2) (2001) 121–138.

[20] P. Ladevèze, A. Nouy, On a multiscale computational strategy with time and space homogeneization for structural mechanics, Comput. Methods Appl. Mech. Engrg. 192 (2003) 3061–3087.

[21] C. Farhat, K. Pierson, M. Lesoinne, The second generation FETI methods and their application to the parallel solution of large-scale linear and geometrically non-linear structural analysis problems, Comput. Methods Appl. Mech. Engrg. 184 (2–4) (2000) 333–374.

[22] A. Klawonn, O. Rheinbach, O.B. Widlund, Some computational results for dual-primal feti methods for three dimensional elliptic problems, in: Domain Decomposition Methods in Science and Engineering, Lecture Notes in Computer Science Engineering, vol. 40, Springer, Berlin, 2005, pp. 361–368.

[23] P. Gosselet, C. Rey, Non-overlapping domain decomposition methods in structural mechanics, Arch. Comput. Methods Engrg. 13 (4) (2007) 515–572.

[24] P. Ladevèze, Nonlinear Computational Structural Mechanics – New Approaches and non-Incremental Methods of Calculation, Springer-Verlag, 1999.

[25] P.-A. Guidault, O. Allix, L. Champaney, J.-P. Navarro, A micro–macro approach for crack propagation with local enrichment, in: Proceedings of the Seventh International Conference on Computational Structures Technology, Lisbon, Portugal, 2004.

[26] P.-A. Guidault, O. Allix, L. Champaney, J.-P. Navarro, A two-scale approach with homogenization for the computation of cracked structures, Comput. Struct. 85 (17–18) (2007) 1360–1371.

[27] P.-A. Guidault, O. Allix, L. Champaney, C. Cornuault, Une approche micro–macro pour le suivi de fissure avec enrichissement local, Rev. Européenne de Mécanique Numérique 15 (1) (2006) 187–198.

[28] I. Babuška, J.M. Melenk, The partition of unity method, Int. J. Numer. Methods Engrg. 40 (1997) 727–758.

[29] G.J. Wagner, W.K. Liu, Hierarchical enrichment for bridging scales and mesh-free boundary conditions, Int. J. Numer. Methods Engrg. 50 (2001) 507–524.

[30] S. Osher, J.A. Sethian, Fronts propagating with curvature-dependent speed: Algorithms based on Hamilton–Jacobi formulations, J. Comput. Phys. 1 (1988) 12–49.

[31] J.A. Sethian, Level Set Methods and Fast Marching Methods: Evolving interfaces in Computational Geometry, Fluid Mechanics, Computer Vision and Materials Science, Cambridge University Press, Cambridge, UK, 1999.

[32] P. Ladevèze, A. Nouy, O. Loiseau, A multiscale computational approach for contact problems, Comput. Methods Appl. Mech. Engrg. 191 (2002) 4869–4891.

[33] A. Nouy, A multiscale computational strategy with space–time homogenization for the analysis of highly heterogeneous structures (in French), Ph.D. thesis, ENS de Cachan, 2003.

[34] F. Brezzi, D. Marini, Error estimates for the three-field formulation with bubble stabilization, Math. Comput. 70 (2001) 911–934.

[35] E. Cosserat, F. Cosserat, Theory of Deformable Bodies, Hermann and Sons, Paris, 1909 (in French).
[36] A.C. Eringen, Linear theory of micropolar elasticity, J. Math. Mech. 16 (6) (1966) 909–923.
[37] L. Champaney, J-Y. Cognard, P. Ladevèze, Modular analysis of assemblages of three-dimensional structures with unilateral contact conditions, Comput. Struct. 73 (1999) 249–266.
[38] R. Glowinski, P. Le Tallec, Augmented lagrangian interpretation of the nonoverlapping Schwartz alternating method, in: Third International Symposium on Domain Decomposition Methods for Partial Differential Equations, SIAM, Philadelphia, 1990, pp. 224–231.
[39] R. Gettu, Z.P. Bažant, M.E. Karr, Fracture properties and brittlened of high-strenght concrete, ACI Mater. J. 87 (6) (1990) 608–618.
[40] T.N. Bittencourt, P.A. Wawrzynek, A.R. Ingraffea, Quasi-automatic simulation of crack propagation for 2D LEFM problems, Engrg. Fract. Mech. 55 (2) (1996) 321–334.